Geophysical Journal International

Geophys. J. Int. (2013) **193,** 557–584 doi: 10.1093/gji/ggt018

Basement inhomogeneities and crustal setting in the Barents Sea from a combined 3D gravity and magnetic model

L. Marello,[1,2,3] J. Ebbing[1,2] and L. Gernigon[1]

[1] *Geological Survey of Norway (NGU), Post Box* 6315 *Sluppen,* 7491 *Trondheim, Norway*
[2] *Department for Petroleum Engineering and Applied Geophysics, Norwegian University of Sciences and Technology (NTNU),* 7491 *Trondheim, Norway*
[3] *Exploro AS, Stiklestadveien* 1, 7041 *Trondheim, Norway. E-mail: laura.marello@exploro.no*

Accepted 2013 January 16. Received 2013 January 15; in original form 2012 May 1

SUMMARY

We present a new 3D geophysical model for the Barents Sea that highlights the basement properties and crustal setting. The model results from the modelling of gravity and magnetic field anomalies and is based on a large number of seismic and petrophysical data. The set up consists of a water layer, sedimentary units that incorporate density variations associated with depth and time of deposition (Cretaceous–Cenozoic, Triassic–Jurassic, Late Palaeozoic and deeply buried sediments), upper and lower basement and an upper mantle. The upper crust is considered as the major source of the magnetic anomalies and has been divided into a number of units characterized by constant densities and magnetization, which show a good correlation with the main structural elements of the Barents Sea. The Southwest Barents Sea crust is an aggregation of allochthonous Caledonian terranes and autochthonous Archaean and Palaeoproterozoic complexes. We interpret the different crustal blocks in terms of distinctive lower, middle, upper and uppermost allochthonous terranes that can be linked with the major nappes onshore. The largest part of the North Barents Sea is distinguished from the rest of the shelf by its low-magnetic properties and its large crustal thickness. These differences are compatible with a geodynamic scenario in which an independent crustal block (Barentsia, not corresponding entirely to the island of Svalbard) was located between Baltica and Laurentia and became attached to the shelf during the Caledonian orogeny. To the east, the basement underlying the large mega-sag East Barents Basin, is an assemblage of Precambrian rocks deformed during the Timanian and Uralian orogenies. The basement is characterized by an alternation of high-magnetic and low-magnetic units that mimic the arcuate shape of Novaya Zemlya. In the Southeast Barents Sea, the crustal units are linked to the onshore geology of the Timan–Pechora region and are mostly the result of Timanian orogenesis.

Key words: Gravity anomalies and Earth structure; Magnetic anomalies: modelling and interpretation; Crustal structure; Arctic region.

1 INTRODUCTION

The Barents Sea represents a large part of the Arctic region and extends between the Norwegian–Greenland Sea, the Arctic Ocean margin, Novaya Zemlya and the Norwegian–Russian mainland (Fig. 1). The geodynamic evolution and crustal setting of the Barents Sea have been in focus for the last few decades due to its petroleum potential (e.g. Johansen *et al.* 1992; Gautier *et al.* 2009; Henriksen *et al.* 2011). Several new regional models have been proposed in recent years (e.g. Ritzmann *et al.* 2007; Barrère *et al.* 2011) discussing the complexity of the area and emphasizing the need for further integrated studies.

The Barents Sea is characterized by structural styles, which differ between the west and the east (Johansen *et al.* 1992; Henriksen *et al.* 2011). The depth-to-top basement in the Barents Sea has previously been estimated in a number of studies (Skilbrei 1991; Johansen *et al.* 1992; Gramberg *et al.* 2001; Ritzmann *et al.* 2007; Barrère *et al.* 2009) that locally point out differences in the order of ±8 km (Marello *et al.* 2010). The large differences can be explained (1) by the difficulties involved in estimating the top of the deeply buried basement using seismic and gravity data and (2) by the definition of the top basement itself. In the deepest basins, sediments are strongly affected by compaction and their densities can approach those of the underlying basement rocks. This results in a decrease of both the acoustic impedance contrast and the signal-to-noise ratio. Furthermore, the presence of salt (e.g. Nordkapp Basin, Svalis Dome) and shallow magmatic intrusions in the basins (e.g. East Svalbard or in Triassic strata in the East Barents Basin) locally complicate the estimation of the depth-to-top basement. The second difficulty is directly related to the concept of top basement. Depending on

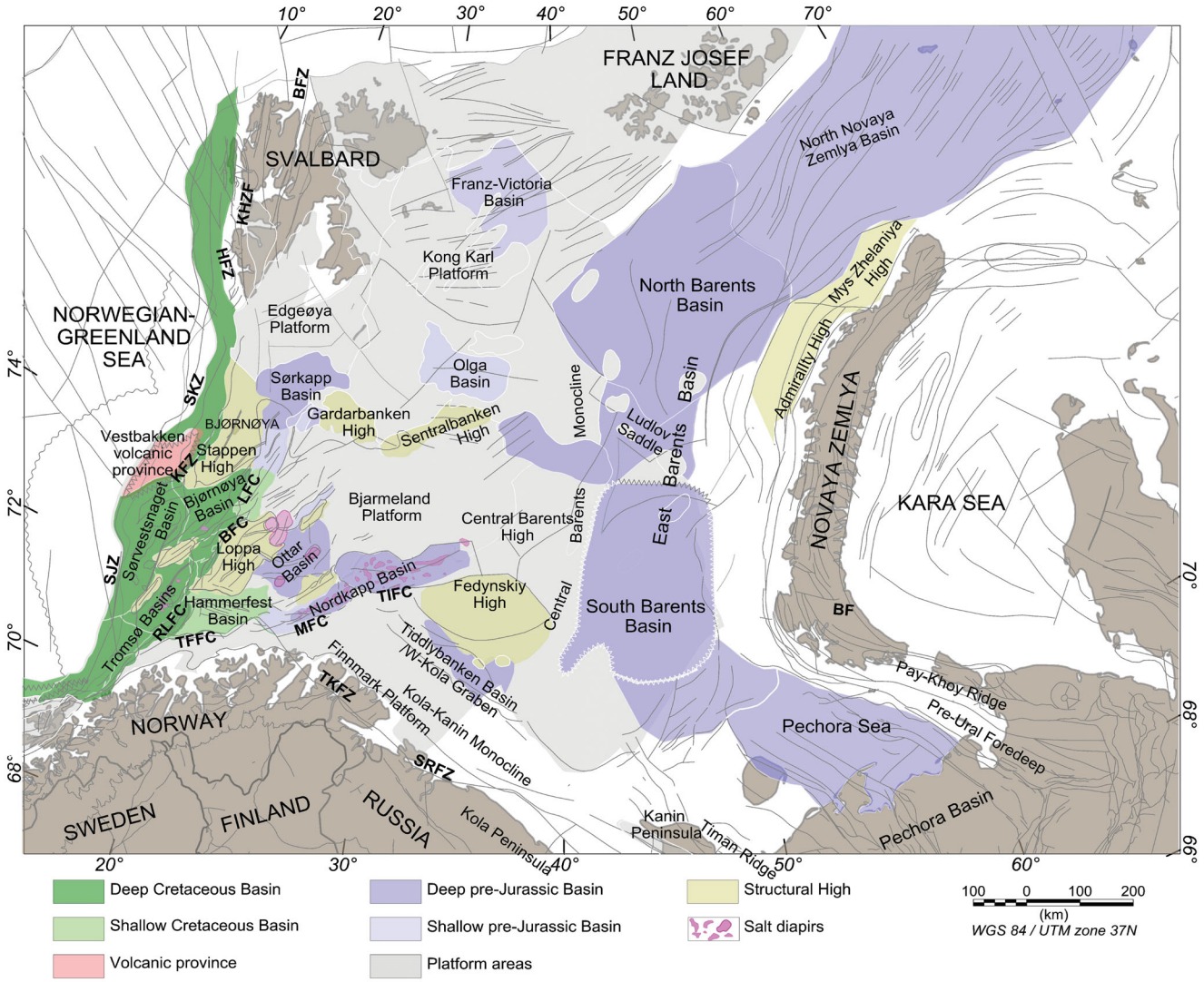

Figure 1. Barents Sea structural physiographic domains with basins, structural highs and platform areas displayed. The abbreviations denote to the major fault complexes: BF, Baidsratsky Fault Zone; BFC, Bjørnøyrenna Fault Complex; BFZ, Billefjorden Fault Zone; HFZ, Hornsund Fault Zone; KFZ, Knølegga Fault Zone; KHFZ, Kongsfjorden–Hansbreen Fault Zone; LFC, Leirdjupet Fault Complex; MFC, Måsøy Fault Complex; RLFC, Ringvassøy–Loppa Fault Complex; SJZ, Senja Fracture Zone; SKZ, Sørkapp Fault Zone; SRFZ, Sredni–Rybachi Fault Zone; TIFC, Thor Iversen Fault Complex; TFFC, Troms–Finnmark Fault Complex; TKFZ, Trollfjorden–Komagelva Fault Zone.

the target of the study area and methods used, the definition and location of the basement surface can be different.

Besides the precise location of top basement surface, location other aspects remain uncertain. The mechanisms involved in basin formation are unknown in many places (e.g. East Barents Basin, Palaeozoic basin locations). The nature of basement also plays an important role in basin initiation and a better understanding of its crustal composition will help us to understand the evolution of the Barents Sea shelf.

As direct offshore sampling and logging of the basement are limited, crustal properties must consequently be studied using indirect geophysical methods. The distributions of densities, susceptibility and seismic velocities allow us to distingush individual areas that can have specific geological histories. In this study, we present a 3D forward model for the entire Barents Sea region, in which we define densities and magnetization for the crust. The model defines the major geometries and allows for a division of the Barents Sea basement into regions with homogeneous properties related to distinctive rock types and geological evolution. The relationship between the nature of the basement blocks, the crustal thickness and basins are discussed in order to provide a better understanding of the evolution of the Barents Sea.

2 THE BARENTS SEA REGION: BASEMENT EVOLUTION

The Barents Sea continental shelf formed by the aggregation of different crustal terranes that evolved during three major orogenic events: Timanian, Caledonian and Uralian. Subsequently, a large number of rifting episodes took place, which led to the complex intracratonic setting that we see today.

The latest Neoproterozoic to Early Cambrian Timanian event involved the Southeast Barents Sea region; the Timan–Pechora Basin, southern Novaya Zemlya and areas offshore in the Barents Shelf (Fig. 1). However, its full extent and significance offshore is still poorly constrained (Olovyanishnikov *et al.* 2000; Roberts &

Siedlecka 2002; Pease & Scott 2009). The Timanian orogenic deformation and metamorphism telescoped and accreted Neoproterozoic magmato-sedimentary assemblages against the northeastern margin of Baltica, generating NW–SE trending, SW-vergent folds and a NE-dipping pervasive cleavage (Roberts & Olovyanishnikov 2004). In this work, the term Timanian basement terranes include the Precambrian sedimentary successions, the volcano–sedimentary and igneous rock units, island arcs and other ocean-floor magmatic rocks involved in the Timanian orogeny.

The western Barents Sea has been strongly influenced by the Caledonian orogeny, which began in the Early Ordovician and culminated with the collision of Laurentia and Baltica in Mid Silurian to Early Devonian time (Roberts 2003; Gee *et al.* 2008). The Caledonian influence is recorded in northwesten part of the West Barents Sea by N–S structural trends and in the southwest by NE–SW structures (Dengo & Røssland 1992; Gudlaugsson *et al.* 1998; Faleide *et al.* 2008), although this last trend is actually now disputed in the light of new aeromagnetic data (Gernigon *et al.* 2008; Gernigon & Brönner 2012). On the Norwegian mainland, the basement is an assemblage of two different types of terrane: the autochthonous rocks of the Fennoscandian Shield (Palaeoproterozoic and Archaean crystalline complexes) and the Caledonian allochthons, which represent the remnants of a Baltoscandian rifted margin system including shelf successions, oceanic and arc units and exotic rocks with Laurentian affinities (Roberts 2003). The allochthons are subdivided into four major groups: lower, middle, upper and uppermost (Roberts & Gee 1985; Siedlecka *et al.* 2004; Gee 2005; Nystuen *et al.* 2008). The Caledonian basement in Finnmark, northernmost Norway extends into the Barents Sea shelf but its nature and geometry beneath the younger sedimentary cover are still not clear (e.g. Ziegler 1988; Doré 1991; Gudlaugsson *et al.* 1998; Ritzmann & Faleide 2007; Faleide *et al.* 2008; Gee *et al.* 2008; Gernigon *et al.* 2008; Barrère *et al.* 2009, 2011).

On the Svalbard archipelago, three crustal blocks can be distinguished. Most authors agree that Svalbard formed the margin of Laurentia in Precambrian and Early Palaeozoic times. During the development of the Caledonides in Silurian time the three domains were united with the rest of the shelf (Cocks & Fortey 1982; Torsvik *et al.* 1996; Hartz & Torsvik 2002; Gee & Teben'kov 2004; Gee *et al.* 2006). Different hypotheses for Caledonian terrane assembly on Svalbard have been suggested and the actual extent of the Caledonide terranes towards the east is controversial (Harland 1985; Harland *et al.* 1997; Gee & Teben'kov 2004; Cocks & Torsvik 2011). The eastern Svalbard terranes have been also interpreted as an old microcrustal block lying between Laurentia and Baltica and later involved in the Caledonian collision (Gudlaugsson *et al.* 1998). Here, we use the term Caledonian basement to comprise all the pre-Carboniferous rocks on Svalbard that form the autochthon and the allochthons involved in the orogeny.

A third orogenic event involving the East Barents Sea—the Uralian event—started in the Early Carboniferous with eastward subduction of the Uralian Ocean beneath the Siberian craton (Churkin *et al.* 1981). The subsequent continental collision between Laurussia (Baltica and Laurentia) and Siberia in the Early Permian produced overthrusting towards the west (Otto & Bailey 1995) and generated the Ural mountain chain. The predominantly west-vergent fold-and-thrust belt on Novaya Zemlya is considered to be the northern extension of the Urals (Otto & Bailey 1995; Puchkov 2002). However, this interpretation is debated due to the large westward offset from the general trend of the orogeny (e.g. Scott *et al.* 2010; Pease 2011). The largest structures in the East Barents Sea reflect the arc-shaped geometry of the island and are attributed to the Uralian deformation (Korago *et al.* 2004). The Uralian basement terrane in our study includes the pre-Carboniferous rocks that were formed at the Uralian margin and the rocks with oceanic affinities that were deformed during the Late Palaeozoic and Early Mesozoic orogeny.

These three collisional events combined to establish the structural framework that controlled the subsequent Palaeozoic and Mesozoic evolution of the Barents Sea (Doré 1991; Johansen *et al.* 1992; Puchkov 2002). The Late Palaeozoic and Mesozoic tectonic history was dominated by several rifting episodes that culminated with the opening of the Norwegian–Greenland Sea (Gabrielsen *et al.* 1990; Johansen *et al.* 1992, 1994; Faleide *et al.* 1993; Smelror *et al.* 2009). In the Early Cretaceous, a significant magmatic event occurred in the northeast of Svalbard (Grogan *et al.* 1998), the intrusions are part of the so-called Arctic Large Igneous Province linking Greenland, Svalbard, Franz Josef Land and adjacent shelf areas (Maher 2001). In addition, numerous Early Cretaceous sills affected the Triassic sediments in the East Barents Basin (Ivanova *et al.* 2011). An additional complexity was provided by the Cenozoic uplift. This event resulted in the emergence of the Svalbard Platform and initiation of erosional processes (Dimakis *et al.* 1998).

The present day Barents Sea is divided into three major structural areas: (1) The West Barents Sea, which is dominated by a complex system of grabens or half-grabens, (2) an extensive platform region which extends towards the eastern and northern parts of the shelf and (3) a large sag basin which occupies the greater East Barents Basin (Fig. 1).

3 DATA

Acquisition of magnetic data in the arctic started already with the early explorers like Nansen (e.g. Smelror 2011). We use gravity and magnetic data, which have been collected over the past 50 yr in many parts of the Barents Sea (e.g. Skilbrei 1991, 1995; Olesen *et al.* 2010; Werner *et al.* 2011). In addition, with the available petrophysical and seismic data, these data sets can be used to describe the crustal structure of the Barents Sea in a consistent way. In the following paragraphs, we describe the individual data sets, which we used for the potential field modelling and interpretation.

3.1 Bathymetry and topography

We use the data of the International Bathymetric Chart of the Arctic Ocean (IBCAO; Jakobsson *et al.* (2008). The model has been compiled using information from contour, grid, point and track data, and has a resolution of 2×2 km. The Barents Sea is not characterized by large depth variations and the sea depth ranges from -40 to -380 m (Fig. 2).

3.2 Gravity data

Gravity data for the area are available from different sources. Here, we use the Arctic Gravity Project (ArcGP) data set (http://earth-info.nga.mil/GandG/wgs84/agp/). The compilation provides free air anomalies. We calculated the complete Bouguer anomaly (Fig. 3a) applying standard corrections (e.g. Blakely 1996). The water depth is replaced with bedrock of a constant density of 2200 kg m^{-3} and the onshore topography with a density of 2670 kg m^{-3}. The standard deviation of the ArcGP is around ± 5 mGal in the West Barents Sea

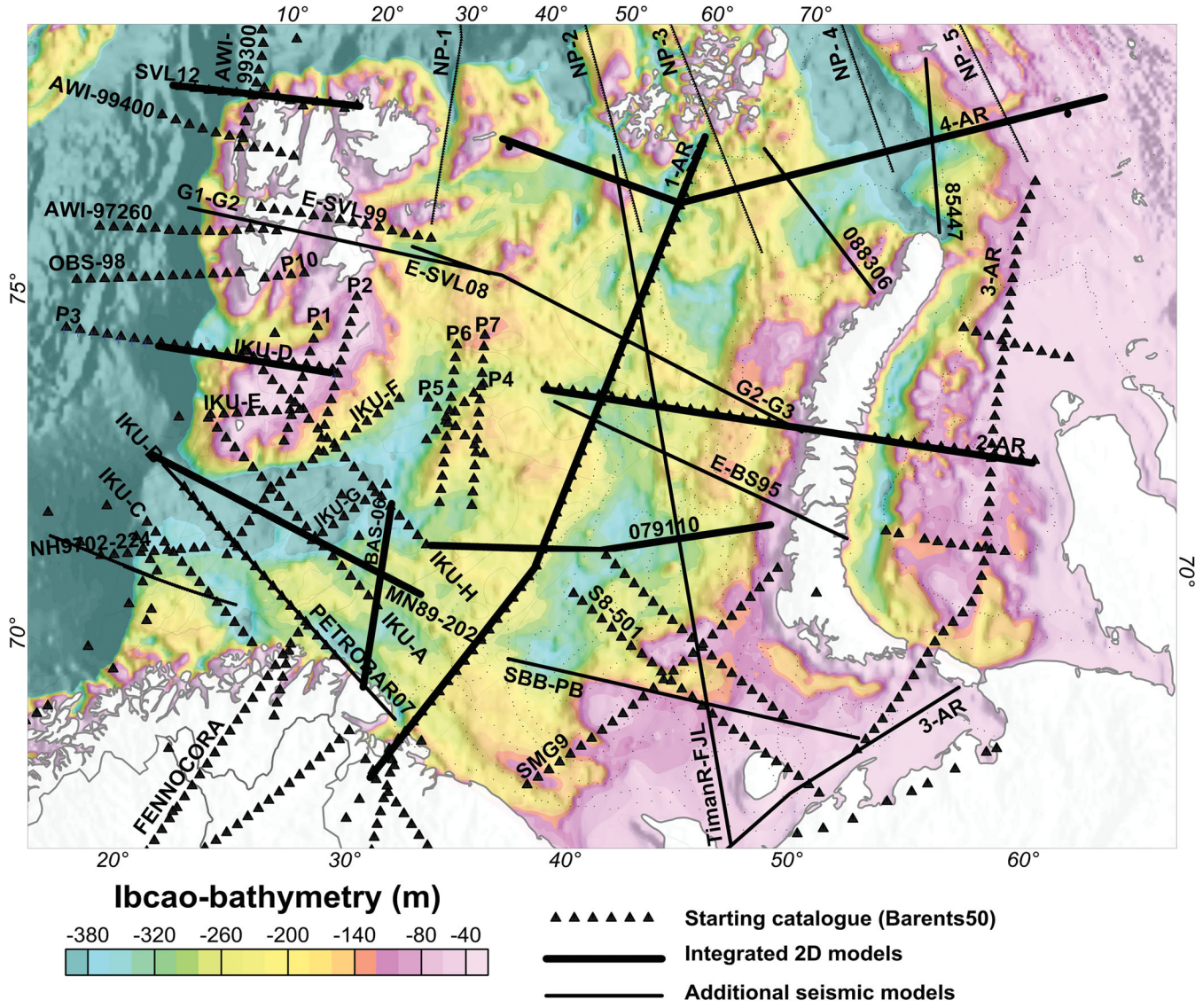

Figure 2. Topography/bathymetry from IBCAO (Jakobsson *et al.* 2008) and location of seismic profiles. Triangles indicate the catalogue included in Barents50 (Ritzmann *et al.* 2007); the thick black lines are regional transects that have been the base for regional models (Marello *et al.* 2010); the thin black lines indicate additional seismic models used in this study (see Table 1 for a complete overview and references).

and Southeast Barents Sea, and around ±8 mGal in the Northeast Barents Sea (Forsberg *et al.* 2007).

3.3 Magnetic data

The magnetic data (Fig. 3b) are based on a compilation integrating released Russian and Norwegian aeromagnetic survey data (Smelror *et al.* 2009; Olesen *et al.* 2010; Werner *et al.* 2011). The mean least square errors of the aeromagnetic surveys are in the order of 11–14 nT (Werner *et al.* 2011).

3.4 Seismic profiles

The seismic data used in this work include both reflection and refraction data, and the horizon interpretation is mostly based on previous publications summarized in Table 1 and shown in Fig. 2. The Southwest Barents Sea is the area with the best coverage of deep seismic profiles. The northwestern boundary of the shelf is covered by data that define most of the sedimentary successions and locally provide information about the seismic top basement. There are a few seismic profiles in the eastern Barents Sea, but the interpretation of the crustal architecture is still controversial. For example, the studies by Ivanova *et al.* (2006, 2011) and Roslov *et al.* (2009) show quite different interpretations along the same seismic transect. Reflectors in the deep crust have been interpreted independently as a shallow Moho (Roslov *et al.* 2009) or as a lens of high-velocity lower crust (Ivanova *et al.* 2006, 2011).

3.5 Regional models

Besides seismic data, a large number of earlier compilations were used to gain insights into the deep crustal geometries and to provide geological and geophysical input during the modelling. Moreover, various horizons have been compiled and used to constrain the geometry of the model. The data are summarized in Tables 2 and 3.

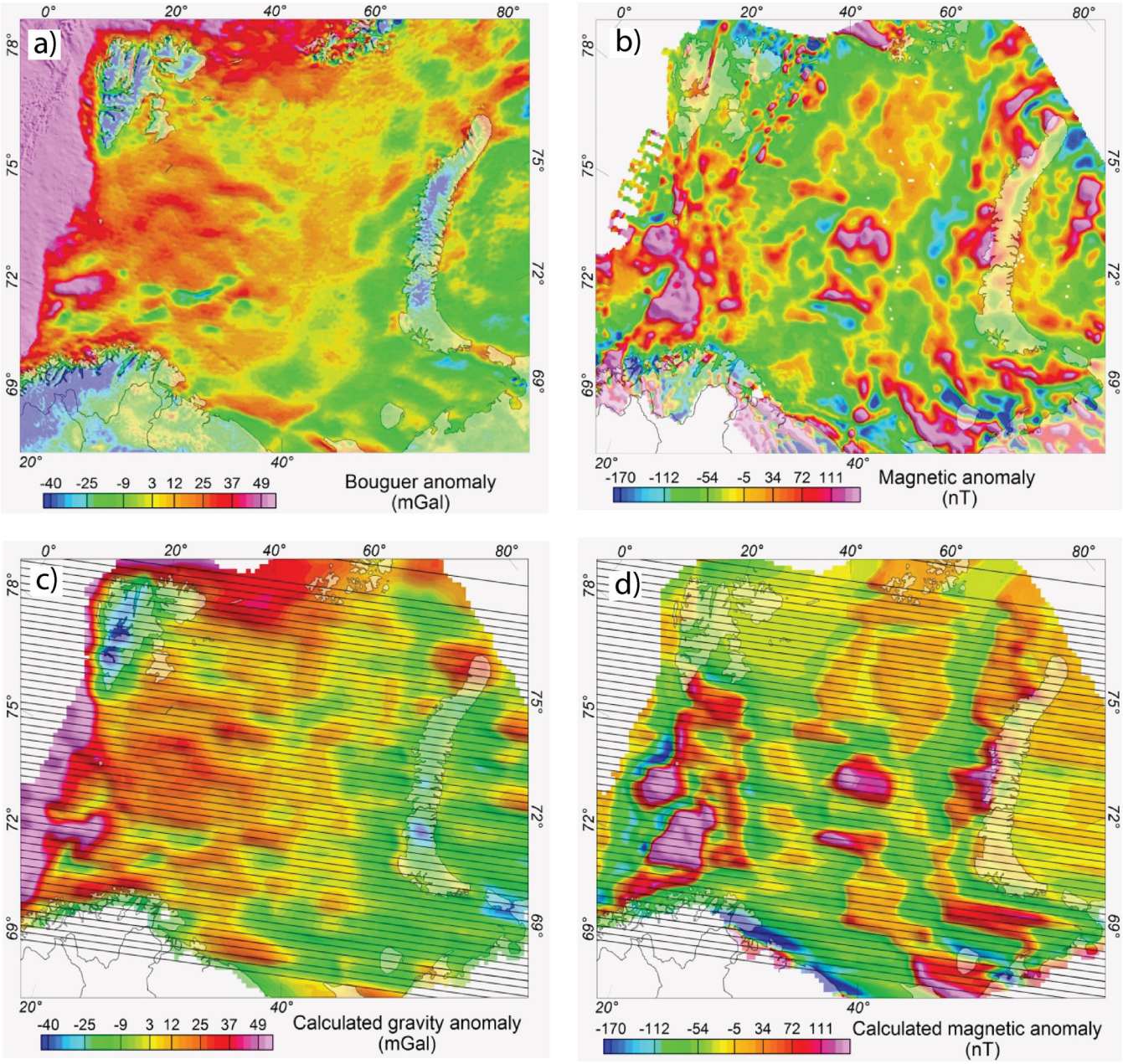

Figure 3. (a) Bouguer anomaly. Reduction density is 2200 kg m^{-3} offshore and 2670 kg m^{-3} onshore. (b) Magnetic anomaly. (c) Modelled gravity anomaly. (d) Modelled magnetic anomaly. Black lines in (c), (d) show the locations of the sections defining the geometry of the 3D model.

A regional seismic velocity distribution for the Barents Sea has been adopted from the Barents50 model, a crustal model based on seismic refraction and seismic reflection profiles in the Barents Sea. The lateral resolution has been estimated at 50 km, and in addition to the velocities the seismic model defines the geometries of three sedimentary and two crustal layers (Ritzmann *et al.* 2007). The crustal model also provides more refined velocity information along the regional seismic profiles with its 25 km sampling distance (Fig. 2).

Depths to the base Cretaceous and top Permian surfaces were provided by Statoil. The base Cretaceous data set covers most of the Barents Sea, while the top Permian covers part of the central Barents Sea and the Southwest Barents Sea. Pre-existing top basement models are available for the western Barents Sea (Skilbrei 1991; Barrére *et al.* 2011), the eastern Barents Sea (Gramberg *et al.* 2001) and for the entire Barents Sea (Johansen *et al.* 1992; Ritzmann *et al.* 2007). The accuracy of the models differs from region to region (Table 3).

For the depth to Moho, we considered two recent compilations: the Barents50 model (Ritzmann *et al.* 2007) and the compilation for the Moho depths of the European Plate (Grad *et al.* 2009). The latter is partly based on Barents50, but extends towards the Baltic Shield and the oceanic domain. The lateral resolution of the new compilation is around 10 × 10 km and the depth uncertainties in the study region are estimated at ±3 km along the edge of the shelf and in the Southwest Barents Sea, and at around ±4 km in the remaining regions.

Table 1. 2D seismic constrains data. The location of the profiles is displayed in Fig. 2.

Seismic lines	Characteristics	References
	West Barents Sea	
NH9702–224	Ocean Bottom Seismometer (OBS)	Mjelde *et al.* 2002
PETROBAR07	OBS	Clark *et al.* 2009
MN89–202	Reflection seismic data (until the top Permian)	Marello *et al.* 2010
IKU-A; IKU-B; IKU-C; IKU-D; IKU-E; IKU-F; IKU-G; IKU-H	Multichannel seismic reflection profiles down to the Moho. Locally combined with OBS.	Gudlaugsson *et al.* 1987; Faleide *et al.* 1993; Gudlaugsson & Faleide 1994; Sanner 1995; Breivik *et al.* 1998; Breivik *et al.* 2003; Ritzmann & Faleide 2007; Barrère *et al.* 2009.
PI; P2; P10	OBS	Breivik *et al.* 2005
P4; P5; P6; P7	OBS	Breivik *et al.* 2002
G1-G2; G2-G3	Combined geological profile	Sigmond & Roberts 2007
OBS-98	OBS	Ljones *et al.* 2004
AWI-97260	Seismic refraction data	Ritzmann *et al.* 2002; Faleide *et al.* 2008
AWI-99400	Seismic refraction data	Ritzmann *et al.* 2004; Faleide *et al.* 2008
AWI-99300	Seismic refraction data	Ritzmann & Jokat 2003
SVL12	Deep seismic experiments	Geissler 2001; Faleide *et al.* 2008
E-SVL99		Høgden 1999
E-SVL08		Minakov *et al.* 2012b
Bas06 seismic lines		Gernigon *et al.* 2008, 2011
FENNOLORA	Long-range seismic refraction profile	Guggisberg *et al.* 1991
	East Barents Sea	
SEbaltica	Deep seismic sounding (DSS)	Kostyuchenko *et al.* 2006
3-AR	Refraction deep seismic and reflection-common-depth point seismic	Ivanova *et al.* 2011
SMG9	Seismic refraction and reflection data.	Gubaidulin *et al.* 1993; Neprochnov *et al.* 2000
S8–501 (DSS-82)	Deep seismic sounding (DSS)	Tulina *et al.* 1988; Morozova *et al.* 2000; Neprochnov *et al.* 2000
079110	Reflection-seismic data (until the top Permian)	Marello *et al.* 2010
TimanR-FJLxyz SBB-PB	Seismic constraint in depth (until the top Ordovician-Silurian)	Johansen *et al.* 1992; Ostisty & Fedorovsky 1993
E-BS 95	Regional seismic profile	Johansen *et al.* 1992; Otto & Bailey 1995
2-AR	Refraction deep seismic and reflection-common-depth point seismic	Ivanova *et al.* 2006, 2011
4-AR	Refraction deep seismic and reflection-common-depth point seismic	Ivanova *et al.* 2011
1-AR.xyz	Onshore and offshore wide-angle reflection/reflaction data. Three components OBS and MCS reflection study. (Refraction deep seismic and reflection-common-depth point seismic)	Sakoulina *et al.* 1999; Verba & Sakoulina 2001; Ivanova *et al.* 2006, 2011
85447; 088306	Seismic constraint in depth (until top Permian)	Shipilov & Vernokovsky 2010
NP-1 NP-2 NP-3 NP-4 NP-5		Minakov *et al.* 2012a
BSWS2009		Ritzmann & Faleide 2009
Linell-EBB Linel5PS	Seismic constraint in depth (until top basement)	Stephenson *et al.* 2006

3.6 Petrophysical indirect estimations

While densities can be indirectly calculated by conversion of seismic velocities to densities, magnetic parameters cannot be estimated from other geophysical data. Only a limited number of studies have presented interpretations of the magnetic field and estimates of magnetic properties (See Table 2).

Table 2. Summary of previous studies which estimated density, velocity and magnetic parameters in the Barents Sea.

		Ottar Basin-Nordkapp Basin	SW-Barents Sea (IKU-C)	Sørvestsnaget Basin (NH9702-224)	SE Svalbard (P4, P5, P5, P7)	Central West Barents Sea (IKU-D)	S Svalbard	SW Barents Sea PERTOBAR07	SW Barents Sea		W Svalbard (AWI-99400)	NW Svalbard (AWI-99300)	W Svalbard (OBS-98)	All Barents Sea	SE-Barents Sea (S8-501; SMG9)	SE-Barents Sea (1-AR-S8-501)	1-AR, 2-AR, 3-AR, 4-AR
		Breivik et al. 1995	Breivik et al. 1998	Mjelde et al. 2002	Breivik et al. 2002	Breivik et al. 2003	Breivik et al. 2005	Clark et al. 2009	Barrère et al. 2009, 2011		Ritzmann et al. 2004	Ritzmann and Jokat 2003	Ljones et al. 2004	Ritzmann et al. 2007	Neprochnov et al. 2000	Morzova et al. 1995	Roslov et al. 2009; Ivanova et al. 2011
Sediments (Cenozoic-Cretaceous)	Vp	1800-2750	1800-2200	1900-4700	3200-4050	1800-4500	3200-3600	1040-4500			1800-3800	>2000	>2900	1800-3600		>2500	>2600
	ρ	1800-2140	1800-2000	2050-2400	>2260	2000-2490			2300-2450		2100-2400	>2000		2050-2590		>2000	2600
	μ								0								0.013
	Q																
Sediments (Jurassic-Triassic)	Vp	3700-4600	3000-5200	5700-5900	4000-4950	4500-5450	4000-5450	4500-5000						4000-5450			
	ρ	2340-2500	2200-2600	2430-2600					2550					2380-2590			2600
	μ								0								0.013
	Q																
Sediments (Palaeozoic)	Vp	5200-5500	>5200		5100-6000	5650-6000	5100-6000	5000			5000-6200	<4800	<4150	4500-6000		<5600	<5800
	ρ	2610-2660	>2600	2620-2750	<2670				2600		2600-2750	<2100 (?)		2640-2710		<2740	2670
	μ								0								0.013
	Q																
Upper Crust	Vp	6000	6100	6200-6900	6300-6700	6000-7000		6000-6500	Caledonian Nappes	Archean-proterozoic	6400-6600	5200-6650	5700-6650	6200-6600	6200-6600	5600-6500	6000-6600
	ρ	2770	2800	2750-2820	2820-2890	2793	2793-2915		2750	2750-2800	2750-2900	2700-2850		2770		2800-2950	2770-2860
	μ								0.0001- 0.01	0.010-0.200							0.006
	Q								Q>1	Q<1							
Lower Crust	Vp	>6600		6900-7900				6500-7000			6700-6900	6300-7000	6600-6800		6600-7000	6300-7300	6600-7200
	ρ	2930		2930	2910-2990	2880			2950		2950-3000	2900-3000				2950-3060	2980-3050
	μ								0.0001								0,126
	Q								0								
Deep crustal body	Vp	>8000		7400										7100-7600			
	ρ	3330							3100					2980-3050			2320
	μ								0.0001								0.088
	Q								0								
Oceanic crust	Vp					6750-7250							3500-7250				
	ρ			2800-2950		2900-2950	2900-2950										
	μ																
	Q																
Mantle	Vp	>8000	>8000		8000-8500	8000		7500			>7900	>8100	7600-8000		8000	> 7700	
	ρ	3330	3200	3180-3220	3330-3450	3240-3330	3330-3340		3300		3240-3300	3300		3300		3320	3320
Mafic intrusion	Vp				6300-6400												
	ρ		3330-3340						3000								2850
	μ								0.015-0.05								0.1
	Q								Q<1								

Vp= P-wave seismic velocity (m/s) ρ= Density (kg/m³) μ= Susceptibility (SI) Q= Königsberger ratio (ratio of remanent to induced magnetisation)

Table 3. Regional layer constraints.

Grid horizons	Resolution	References
Bathymetry (IBCAO)	2 km	Jakobsson *et al.* 2008
Base Cretaceous	0.5 km	Statoil
Top Permian	2 km	Statoil
Top basement all Barents Sea (Barents50)	50 km	Ritzmann *et al.* 2007
Top basement all Barents Sea	?	Johansen *et al.* 1992
Top basement West Barents Sea	5 km	Skjlbrei *et al.* 1991
Top basement West Barents Sea	>10 km	Barrère et al 2011
Top basement East Barents Sea	?	Gramberg *et al.* 2010
Moho (Barents50)	50 km	Ritzmann *et al.* 2007
Moho	10 km	Grad *et al.* 2009
Moho W-Barents Sea	>10 km	Barrère *et al.* 2011
Barents 1D	25 km on profiles	Ritzmann *et al.* 2007

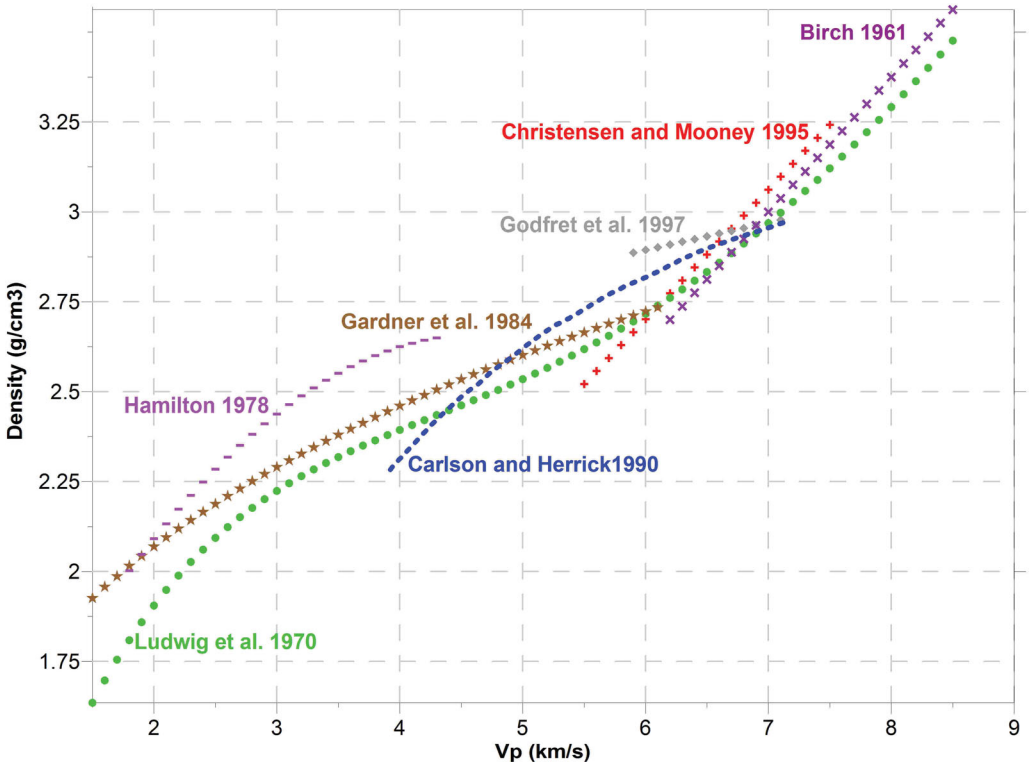

Figure 4. Summary of velocity–density relations. Their application is limited to a certain type of rock as follows: Ludwig *et al.* 1970 for sedimentary and crystalline rocks; Larsen *et al.* 1994 for shale rocks; Gardner *et al.* 1984 for sedimentary rocks; Carlson & Herrick 1990 for oceanic crust; Godfrey *et al.* 1997 for basalts, diabase and gabbros; Christensen & Mooney 1995 for crystalline rocks and Birch 1961 for diabase, gabbro and eclogite rocks.

Initial density estimates are made from conversion of velocities from seismic refraction and reflection studies to densities using empirical relations as presented in Fig. 4. Depending on the relationship used and the type of basement rock, very different densities can be estimated for the same velocity.

Table 2 provides a summary of seismic velocities, densities and magnetic parameters used in previous studies. In Fig. 5, we organize the density and seismic velocity values according to their lithology and geographic location. For sedimentary layers the variations are relatively large, which reflects the gradual increase from top to bottom within each layer. Such an increase is mostly explained by increased sediment compaction with depth (e.g. Athy 1930). In the basement the density range is more limited, and regional differences can be observed. Crust densities versus velocities are plotted in Fig. 5b and a general increase of densities occurs with an increase of velocities, but no simple linear or exponential relationship can be established. To find a statistically meaningful relationship more sample points would be needed.

3.7 Petrophysical samples

Petrophysical data from samples or boreholes are sparse for the Barents Sea. Samples of the sedimentary layers are available from well data (e.g. Tsikalas 1992; Dibner 1998), which confirm the density increase with burial depth. Only a few measurements of the offshore basement density exist (Dibner 1998; Slagstad *et al.* 2008), while for onshore Norway a large database has been established from abundant rock samples (e.g. Olesen *et al.* 2010). A distinction between some of the Caledonian nappes can be made between rocks of the higher density Upper Allochthon (2800–2850 kg m^{-3}) and the lower density lower, middle and uppermost allochthonous terranes

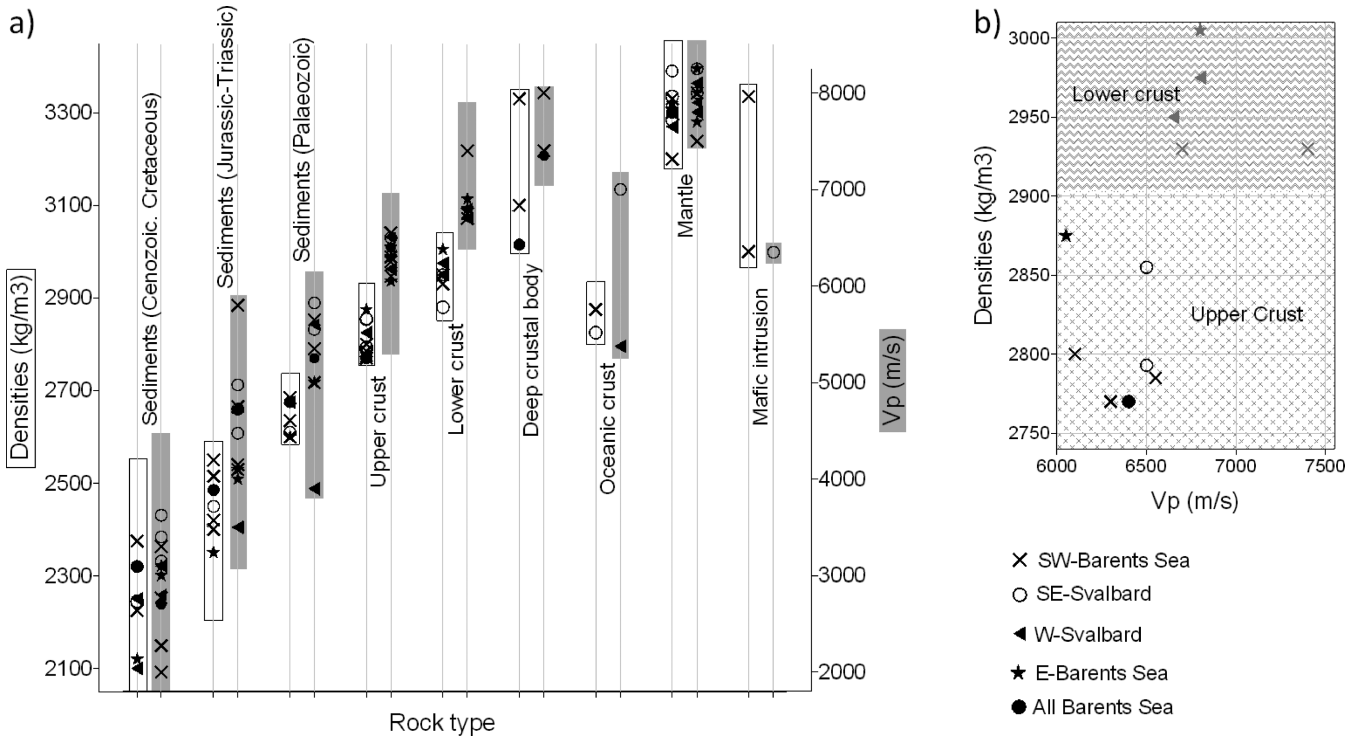

Figure 5. Densities and velocities from previous models (see Table 2). (a) Each symbol corresponds to an average value estimated from the available literature. The data are classified by regions and by rock type. The white boxes represent the density range; the grey the seismic velocities range. (b) The upper crust and lower crust densities are plotted versus velocities.

(2650–2750 kg m^{-3}). Densities of the autochthonous terrane are established to be around 2700–2800 kg m^{-3}.

A few susceptibility and remanence measurements of the basement are available for the western Barents Sea (Åm 1975; Olesen *et al.* 1990, 2010; Skilbrei 1991; Slagstad *et al.* 2008) and for Franz Josef Land (Dibner 1998).

From onshore data, one can establish average magnetic properties for the Caledonian terrane and extend the results to the offshore domain. The autochthonous Archaean and Palaeoproterozoic complexes have extremely high magnetic properties (>0.01 SI), whereas the Lower Allochthon is non-magnetic (<0.0003 SI), the Middle Allochthon is poorly magnetic (0.001–0.003 SI) and the Upper and Uppermost allochthons are moderately magnetic (0.001–0.01 SI; Olesen *et al.* 2010). Magnetic properties for sediments in the offshore domain have been reported only for the West Barents Sea (Dibner 1998; Olesen *et al.* 2010) and are up to two orders of magnitude lower than those of the magmatic and metamorphic rocks forming the basement. Magnetic measurements for Uralian and Timanian basement rocks are not available. For these regions, we adopt average susceptibilities that consider the estimated values for the western Barents Sea and the general petrophysical data for basement rocks (Hunt *et al.* 1995; Clark 1997).

Remanent magnetization has been measured for the crystalline bedrock of Norway (Slagstad *et al.* 2008; Olesen *et al.* 2010) and the direction of the natural remanent magnetization was, in general, found to be parallel to the direction of the present-day Earth's field. The *Q*-values (*Königsberger* ratio of remanent to induced magnetization) are generally low (in the order of 0.5), but mafic and ultramafic rocks commonly show high *Q*-values. On Franz Josef Land (Fig. 1), the few measurements of remanent magnetization that have been published (Dibner 1998) show high remanent magnetization for igneous rocks, dykes and associated basaltic sheets and sills. The observed vector direction of remanence in basalts and dolerite coincides with the present-day magnetic field direction.

4 THE MODELLING PROCESS

An integrated forward modelling process is adopted in this study. Gravity and magnetic fields are modelled simultaneously, and are constrained by seismic profiles and petrophysical data. Modelling has been carried out using the IGMAS (Interactive Gravity and Magnetic Application System) modelling package (Götze & Lahmeyer 1988; Schmidt & Götze 1998, 1999). IGMAS uses polyhedrons with triangulated surfaces as an approximation for the complex 3D geology. A constant density, susceptibility and remanent magnetization are ascribed to each polyhedron. The geometry is defined along parallel vertical sections with a separation of 25 km in the study area (Figs 3c and d). IGMAS triangulates the geometry between the sections and calculates the potential field effect of the model at a designated station location. Afterwards, the model is adjusted by matching the modelled field effect to the observed data by trial and error.

In order to use absolute densities, a reference model was constructed to represent the density of the lithosphere. The reference model was defined by three layers: the upper crust (from 0 to −15 km: 2670 kg m^{-3}), the lower crust (from −15 to −32 km: 2850 kg m^{-3}) and the upper mantle (from −32 to −300 km: 3270 kg m^{-3}). This reference model reflects the average structure of the regional Barents50 model (Ritzmann *et al.* 2007).

For the calculation of the magnetic field, we defined a geomagnetic reference field based on the Definitive Geomagnetic Reference Field (DGRF). Over the Barents Sea, the magnetic field is varying in total intensity (53 500–57 000 nT), declination (5°–35°) and inclination (79°–85°). For the model, we considered a regional mean

value of total intensity of 55 000 nT, with a declination of 18.5° and inclination of 81°. The use of a variable magnetic reference field affects the regional characteristics of the calculated fields only to a minor degree. Magnetic anomalies reduced to the pole, often, are used to avoid the complex calculation of the anomalies using the non-vertical Earth magnetic field. We estimated differences between calculated anomalies using a mean value of the reference field in one case and continuous magnetic anomalies reduced to the pole in another case, and discrepancies were around ∼2 nT. This error is very small as compared with the uncertainties of the final model.

4.1 Initial model set up

The initial model consists of three different sedimentary layers, two crustal layers and the mantle. The first calculated field from the initial model was quite different from the observed field. To improve the fit, we first refined the geometry in order to constrain the structure of the crust as well as the existing data would allow, and then we interactively adjusted the model.

4.2 Sedimentary cover

The upper boundary of the model, bathymetry, was taken from Jakobsson *et al.* (2008) (Fig. 2) and the geology on the seabed is based on the geological map in Sigmond & Roberts (2007). The continent–ocean transition zone (COT) was delineated from the analysis of the magnetic anomaly pattern.

The geometrical and sedimentary setup considers the major seismic horizons (Table 3) and has been refined in a second phase along the available 2D seismic lines (Table 1 and Fig. 2). The density distribution in the sedimentary basins can be related to compaction, grain composition, time of deposition and metamorphic grade (e.g. a change from greenschist to amphibolite facies). In our model we study the influence of two dominant parameters, age and burial depth, as described below.

Two major reflectors can be traced regionally in the Barents Sea, the base Cretaceous and the top Permian. These boundaries correspond to a clear velocity contrast and density change. Accordingly, we define sedimentary units with constant densities corresponding to (1) the Cretaceous–Cenozoic, (2) the Jurassic–Triassic and (3) the Late Palaeozoic successions. In addition, a deep sedimentary body has been introduced in the model in the East Barents Basin at depths below approximately 10–12 km, where burial metamorphism is considered to have significantly altered the physical rock properties. Therefore, the use of the constant Palaeozoic sediment density was not logical here. For the same reason, the Cenozoic–Cretaceous sedimentary package of the West Barents Sea has been divided into an upper and a lower unit in the deepest sedimentary basin (Bjørnøya Basin, Tromsø Basin, Sørvestsnaget Basin). Fig. 6a shows the gravity contribution of the sedimentary layers so defined. The densities for each sedimentary unit are given in Table 4.

Fig. 6b displays the gravity effect of a sedimentary cover with densities defined according to burial depth. In this alternative model, the densities changes due to compaction, sediments at the same depth have the same density. In the uppermost 4 km the sediment density increases with depth as observed in borehole data (Tsikalas 1992). For the sediments between 4 and 6 km, the increase of densities with depth has been extrapolated, and for the deepest sediments a constant value of 2690 kg m^{-3} has been applied. This compaction model with exponential increase of density with depths is strongly simplified for the Barents Sea, as uplift and erosion have affected the sedimentary basins. A lateral increase of density is expected and is related to the amount of erosion.

Both setups produce a gravity effect that is strongly influenced by the total thickness of the sedimentary successions. However, the gravity effect of the first model (Fig. 6a) is more sensitive to the internal discontinuities associated with the principal seismic reflectors. Large negative anomalies occur over the deep Jurassic basins (e.g. Tromsø Basin, Sørvestsnaget Basin, Ottar Basin and Nordkapp Basin), and over the East Barents Basin, while larger positive anomalies are located on structural highs (e.g. Stappen and Loppa Highs). The second model produces smaller anomalies that are, in general, less sensitive to the sedimentary thickness (Fig. 6c). Below 6 km depth, the density of the sedimentary layers is almost identical to the underlying basement, producing almost no contrast and no significant gravity effect. This can be clearly seen in the gravity difference between the two approaches (Fig. 6c). The largest difference is associated with the deepest basins (e.g. East Barents Basin, Nordkapp Basin).

Consequently, we performed some sensitivity tests to estimate the impact that different density distributions in the sediments could produce on crustal geometries. In these tests the gravity differences obtained by the two approaches (Fig. 6c) were considered as gravity residuals to be explained by crustal thickness variations. We estimate that differences of 20 mGal, (Fig. 6c) affect the modelling in terms of crustal thickness by around 5 km.

4.3 The crustal model

The modelling of the crust was the main focus of this work, and in particular we aimed at defining the crustal geometry and its properties.

Top basement and Moho were defined following the pre-existing regional models (Table 3) and later refined by incorporating 2D seismic profiles (Table 1 and Fig. 2). The distinction between upper and lower crust was introduced depending on the reflectivity and velocities from the seismic profiles (Table 1 and Fig. 2). The crossing points of the original profiles show some disagreements due to the accuracies of the different techniques and modelling approaches used. At those points the definition of the geometry was guided by the potential field residuals and designed in such a way to be coherent with the neighbouring setting.

The Barents Sea shelf is characterized by a relatively small range of gravity anomalies ±40 mGal (with the exception of the Loppa and Stappen highs) that show a good correlation with the distribution of basins in the West Barents Sea (Figs 1 and 2a). However, in the East Barents Sea, where the large sag basin is located there is no correlation with the observed negative gravity anomaly. This situation could imply either that no density contrast exists between the lower part of the sedimentary package and the basement, or that the low densities in the basin are isostatically compensated by high densities in the crust (e.g. shallow Moho or high-density lower crust). This ambiguity in interpreting the density distributions could be partly solved by the use of magnetic field. Sedimentary compaction does not alter the magnetization significantly and, consequently, the sediment/basement magnetic contrast remains a detectable magnetic boundary.

For that reason, our initial subdivision of the crust into different basement units has been based on a first interpretation of the magnetic anomalies (Marello *et al.* 2010). The magnetic anomalies of

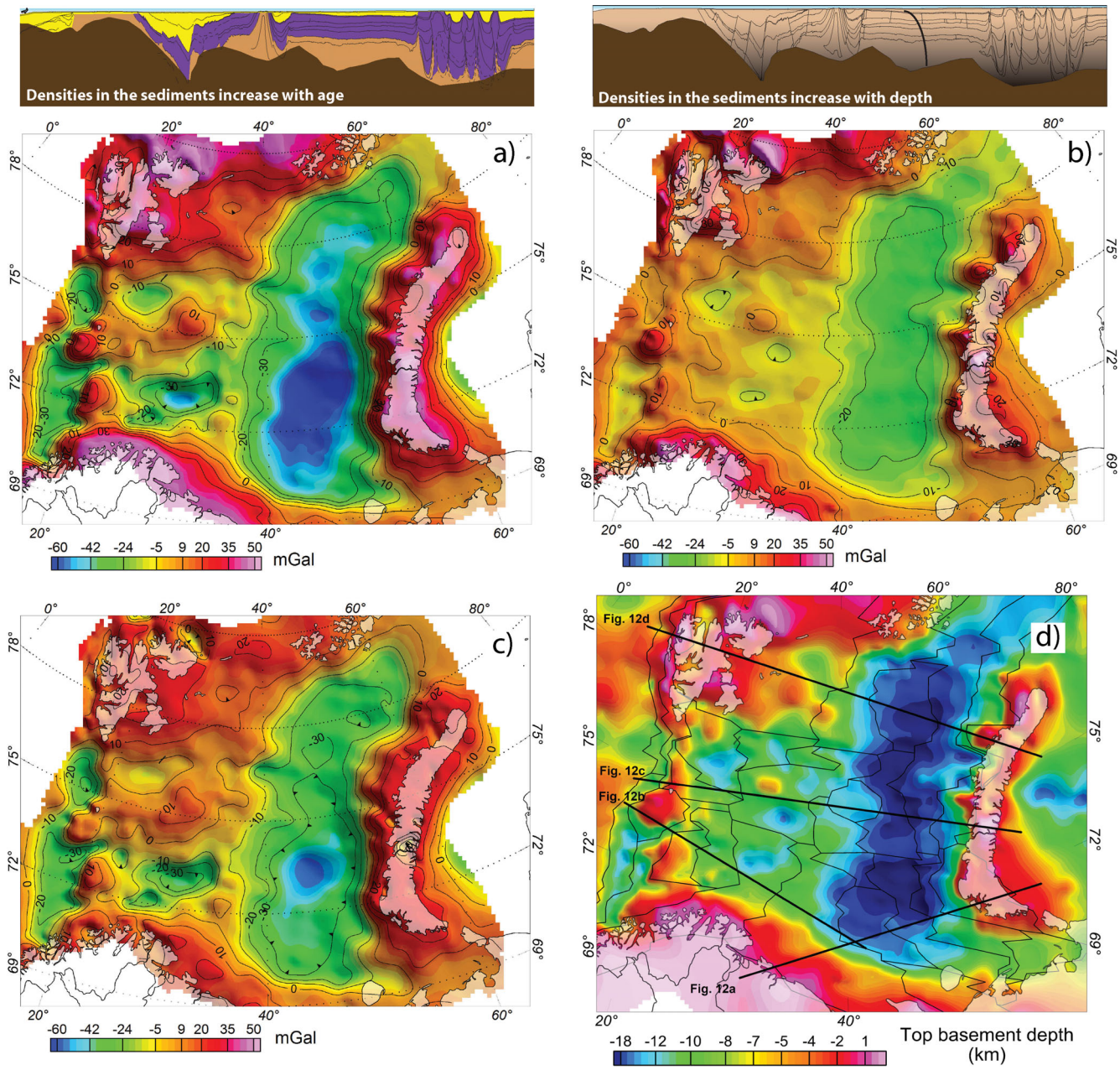

Figure 6. Gravity contribution of the sediments: (a) calculated using densities that increase with age of the sedimentary cover. Constant densities are used for sediments with the same age (yellow = Cretaceous–Cenozoic, purple = Jurassic–Triassic and light brown = Late Palaeozoic); (b) calculated using depth-dependent densities. Constant densities are used for sediments at the same depth. (c) Differences between the gravity effect of the sediments calculated in the two set ups. (d) Top basement model with the outline of the upper crustal blocks. See text for details.

Table 4. Petrophysical model results.

Model unit	Density kg m^{-3}	Susceptibility (SI)	Q ratio (SI)
Cenozoic–Cretaceous sediments (upper and lower)	2350–2450	0	0.3–0.4
Jurassic—Triassic	2500	0	0.3
Palaeozoic	2650	0	0.3
Deep sediments	2730	0	0.3
Oceanic Crust	2850	0.006	2.5
Continent–oceanic transition crust	2750–2800	0.01–0.003	0.5
Upper crust (28 blocks)	2715–2840	0.029–0.00004	0.3–1.5
Lower crust (3 blocks)	2940–3000	0.007–0.00006	0.4
Lower crustal body	3050	0	0
Upper mantle	3280	0.003	0
Rift anomaly mantle	3220	0	0

the Barents Sea, besides being sensitive to the top basement geometry and sedimentary/basement contrast, are influenced mainly by the magnetic properties of the upper crystalline crust (Marello *et al.* 2010).

The magnetic field modelling was focused on fitting general trends to the magnetic signature, and neglecting high-frequency anomalies generated by intrasedimentary sources (e.g. sill intrusions). For each magnetic domain defined by Marello *et al.* (2010) a density value has been attributed, taking into consideration existing seismic velocity and density models (see Table 2 and Figs 4 and 5).

The final organization of the basement blocks derives from the results of tested and modified model set ups and simultaneously reducing the gravity and magnetic residuals. To this end, we managed to create a simple crustal organization that was compatible with all the geophysical constraints. The lateral boundaries of the different domains were considered to have a large degree of freedom, whereas the top basement and Moho were modified only where no constraints existed.

A lower crustal body has been defined (Fig. 8b) based on seismic results beneath the East Barents Basin (Ivanova *et al.* 2006, 2011) in order to evaluate the different theories regarding the deep crustal setting of the East Barents Sea (see section 5.3).

4.4 Regional long-wavelength gravity model: upper mantle density variations

The long-wavelength gravity anomalies are mostly attributed to the crustal thickness and the density distribution in the uppermost mantle. The regional gravity anomalies highlight a strong regional E–W trend attributed to the continental break up and spreading of the North Atlantic Ocean. If a homogeneous upper mantle is assumed, the calculated gravity field is much larger on the oceanic side than the observed gravity anomalies. A range of different approaches has been used to explain that misfit (e.g. O'Reilly *et al.* 1998; Breivik *et al.* 1999; Kimbell *et al.* 2004, 2010; Ritzmann & Faleide 2009).

We address this issue here by means of an oceanic mantle body that approximates the mantle change from a continental to an oceanic domain. Its upper part accounts for the density decrease related to lateral temperature variation (Breivik *et al.* 1999; Kimbell *et al.* 2004), while its lower part reflects a negative velocity anomaly observed on seismic tomography (Levshin *et al.* 2007). The densities of the oceanic mantle are chosen based on petrophysical models (e.g. Bonatti & Michael 1989). Remaining long-wavelength gravity residuals over the shelf are accredited mostly to the Moho geometry and have been addressed by adjusting this surface within the range of the uncertainties provided by the seismic model (Fig. 10d).

5 MODELLING RESULTS

The densities and magnetic properties of the final model are summarized in Table 4. To reduce the ambiguity in potential field modelling, the integration of a large number of data that constrain the geometry or physical model parameters is of fundamental importance. The model presented was defined progressively with a careful iterative stepwise modelling procedure. We mostly rely on the accuracy of the constraints and on the geological meaning of the model to avoid an overfitting of the observed anomalies. The largest uncertainty in the model remains in the northern part of the shelf. The basement blocks defined between Svalbard and Franz Josef Land are quite large. Refinements to these blocks are limited due to a lack of geophysical constraints and the difficulty in determining precisely the shallow sources (sills and dykes) responsible for high-frequency anomalies.

The sedimentary cover is defined by units with constant densities and almost non-magnetic properties, and with a geometry, which is based on the identified major seismic reflectors. Each sedimentary unit is characterized by sediments of similar age (Table 4). On the continental shelf, upper and lower crusts have been distinguished. The spatial extension of the upper crustal units and their physical properties are presented in Fig. 7. The densities clearly differentiate the West Barents Sea (dominated by lower densities) from the East Barents Sea (dominated by higher densities). The magnetic property

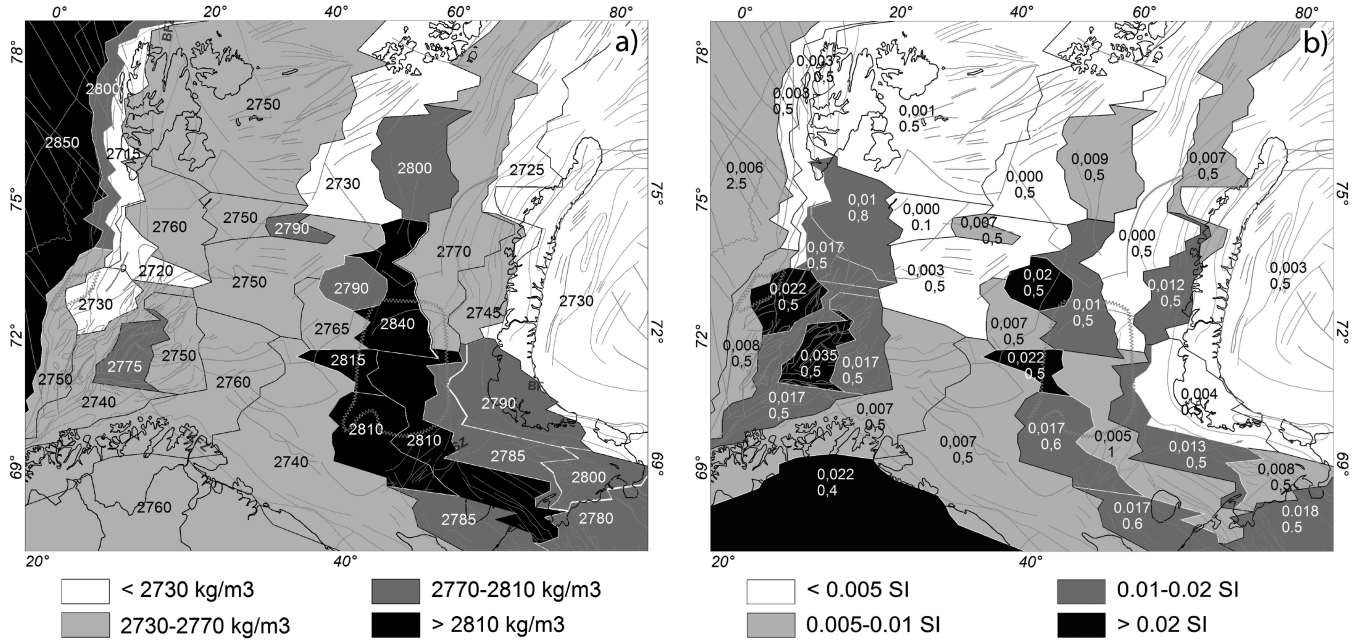

Figure 7. Upper crustal properties: (a) density distribution; (b) magnetic susceptibilities (upper number) and *Q*-ratio (Königsberger ratio) (lower number).

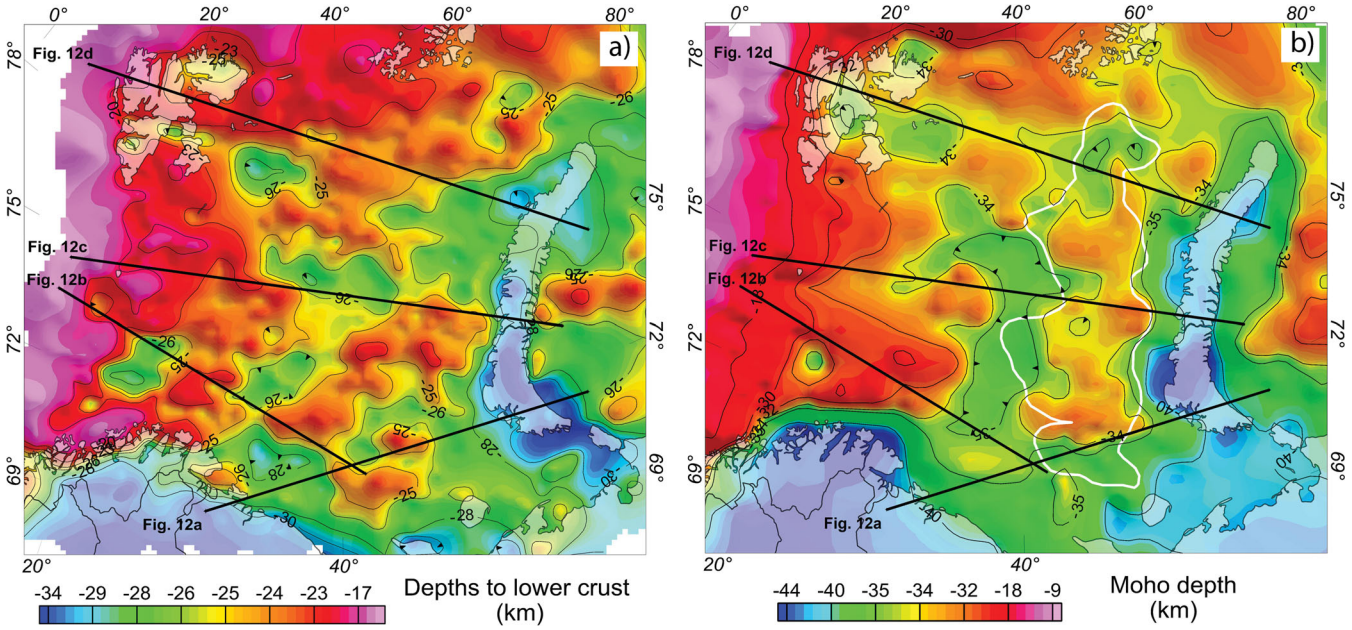

Figure 8. Crustal model: (a) upper–lower crust boundary; (b) Moho depth. The white line shows the outline of the lower crustal body.

distribution in the upper crust allows us to differentiate three major areas: (a) a higher magnetic basement in the Southwest Barents Sea; (b) a non-magnetic crust in the northwestern part of the shelf and (c) an alternation of magnetic and non-magnetic blocks under the East Barents Sea Basin. Towards the margin, a transitional crustal block and the oceanic crust are defined from the bottom of the sedimentary cover to the Moho (Fig. 8).

The lower crust is divided into three blocks. The densities are slightly lower for the two western blocks (2940 kg m^{-3}) than for the eastern lower crust (3000 kg m^{-3}). The magnetic properties are close to zero for the East and Northwest Barents Sea areas, while the Southwest Barents Sea has a magnetic lower crust (with a susceptibility of around 0.005 SI).

The final calculated gravity field (Fig. 3c) has a correlation coefficient of 0.88 with the observed field (Fig. 3a) and a standard deviation of ±11.5 mGal. This is higher than the accuracy of the gravity compilations (Forsberg *et al.* 2007), but if we consider only the wavelengths within the resolution of our model, the fit is reasonably good. Local structures (e.g. salt diapirs in the Nordkapp Basin; sill intrusions to the east of Svalbard) cannot be addressed properly with the set up of our regional model. The largest gravity differences between calculated and observed fields are located onshore Svalbard and Novaya Zemlya, and these may be attributed to local near-surface density variations or they could represent an effect of permanent ice cover not incorporated in the model. The ice cover can locally have an effect in the order of 30 mGal, with a maximum of 45 mGal over the islands of Svalbard and Novaya Zemlya (e.g. Ebbing *et al.* 2007). The calculated magnetic field of our model explains, with a reasonable fit, the observed regional anomalies (Figs 3b and d). The long-wavelength anomalies are modelled assuming a basement origin; short-wavelength anomalies associated with intrabasement magnetic sources would require a detailed modelling of local structures which is too complex to incorporate in the current regional model. The four largest magnetic anomalies located over the Loppa High, the Stappen High and the double anomaly over the central part of the Barents Sea are all well reproduced by the model. In the northwestern part of the Barents Sea, high-frequency magnetic anomalies are observed and are most likely related to intrasedimentary magmatic intrusions (Grogan *et al.* 1998). These particular anomalies make it difficult to distinguish between local and regional magnetic anomalies and thus complicate the modelling and interpretation in this region.

The final 3D model set up is displayed in Figs 6c, 7, 8 and 11. The model defines densities and magnetic properties for the crust and upper mantle, as well as key crustal horizons for the region, that is, the crust–mantle boundary (Moho), top of the lower crust, top basement and the major boundaries of sedimentary successions (Figs 6d and 7). Thickness maps have been calculated from the model and are shown in Fig. 9.

5.1 Depth-to-top basement

The boundary between sediments and basement in our model coincides with a seismic velocity jump recorded along 2D lines and a density contrast from +50 to +200 kg m^{-3} (depending on the age of the sedimentary strata and the basement type). The top basement from density modelling and seismic interpretations almost coincides with the uppermost limit of the magnetic sources, suggesting a surface close to the real crystalline basement.

The top basement map (Fig. 6d) reflects the structural setting of the entire continental shelf. The Southwest Barents Sea is dominated by large variations in the top basement geometry. Two major structural highs, the Loppa High and Stappen High, are recognized where the basement rises to a depth of 2–3 km and crops out on Bjørnøya. Depths to basement reach almost 12 km beneath the Harstad–Tromsø Basin, Sørvestsnaget Basin, Nordkapp Basin and Sørkapp Basin and in the southern part of Sentralbanken High. In the Northwest Barents Sea, the basement is relatively flat and shows maximum depths of *ca.* 8 km. In proximity to the Svalbard archipelago, the basement is quite shallow cropping out locally (northeast of Svalbard and west of the Kongsfjorden–Hansbreen Fault Zone (KHZF in Fig. 1, Harland *et al.* 1997; Gee & Teben'kov 2004)).

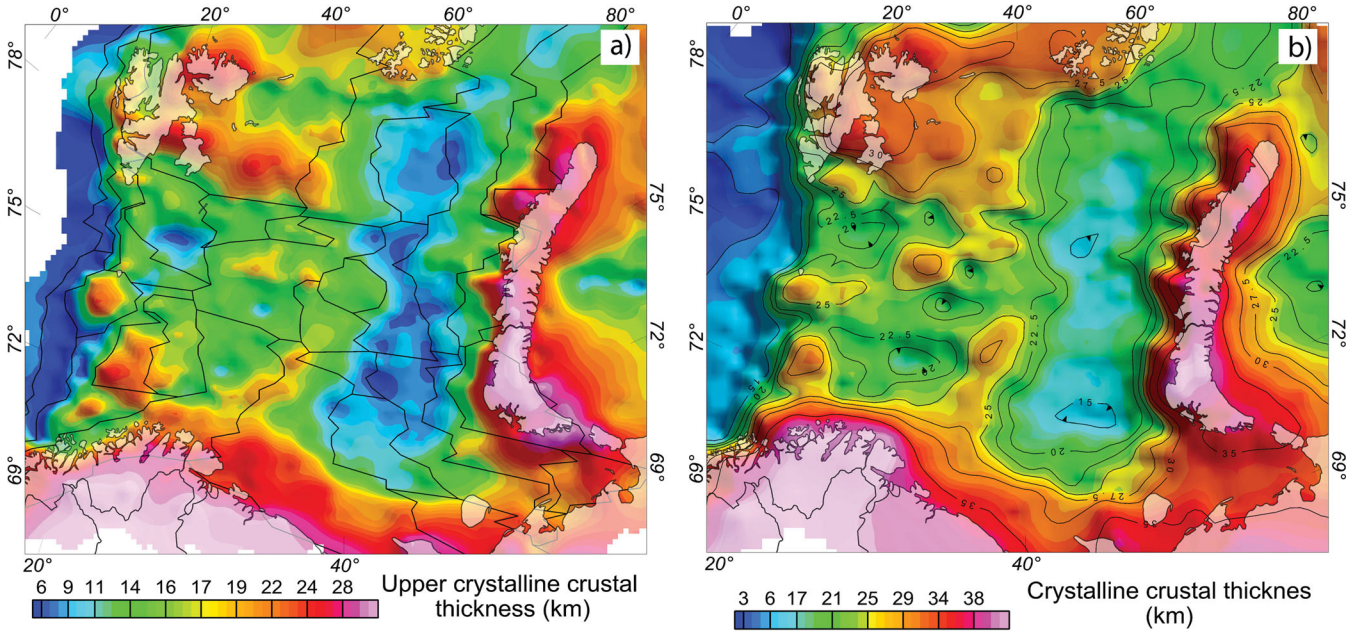

Figure 9. Basement thickness maps. (a) Upper-crystalline crustal thickness map with the outline of the upper crustal blocks; (b) total crystalline crustal thickness map (from top basement to Moho).

In the eastern Barents Sea, the basement geometry follows a unique and large regional structure; the East Barents Basin with a maximum depth reaching more than 18 km.

5.2 Boundary between upper and lower crust

The boundary between upper and lower crust (Fig. 8a) coincides with a jump in seismic velocities, a density contrast of +150 to +220 kg m^{-3}, and a decrease in the magnetic properties in our model.

The geometry of this boundary is fairly flat with depths in the range 22–28 km. The top of the lower crust is locally relatively deep, for example, in proximity to the Loppa High, below the Kola–Kanin Monocline, to the southeast of Svalbard, and beneath Novaya Zemlya and the Pechora Basin, whereas it is shallower in the western and northern parts of the shelf.

5.3 Lower crustal body

A lower crustal body has been inferred to exist beneath the Barents Sea Basin in order to validate the seismic interpretations that proposed either a lens of 'mantle mixture' in the lower crust (Ivanova *et al.* 2006, 2011) or an uplift of the mantle under the basin (Roslov *et al.* 2009). Fig. 8b displays the location of the body. The density of this body (3050 kg m^{-3}) is similar to that of the lower crust (3000 kg m^{-3}), and its thickness is in the order of 1.5 km up to a maximum of 2.5 km. These characteristics make the existence of the proposed body doubtful and almost insignificant in terms of gravity modelling, as such a small density contrast is below the resolution of the model and within the range of uncertainties of seismic interpretation.

5.4 Crust–mantle boundary (Moho)

The modelled Moho depth (Fig. 8b) reaches a maximum beneath the Fennoscandian mainland (40–45 km) and southern Novaya Zemlya (45 km). The Moho is relatively shallow in the western Barents Sea where it rises to a minimum depth of 12 km, reflecting the transition from the continental shelf to the oceanic domain. Despite this large variation, the depths to Moho over the Barents Sea shelf are fairly uniform. In the Southwest Barents Sea, the depths are around 30–33 km with a local deepening below the Loppa High down to 35 km. In the northwestern areas and in the East Barents Sea, the crust–mantle boundary is located at 33–37 km depth. Beneath the mega-basin of the East Barents Sea, our model suggests a 2–3 km shallowing of the mantle.

5.5 Basement thickness (upper crustal thickness and total crystalline thickness)

Two different thickness maps have been calculated from the model. The first represents the thickness of the upper crust, which gives the strongest contribution to the magnetic anomalies (Fig. 9a). The second map represents the crystalline crustal thickness from top basement to Moho (Fig. 9b). The mean crystalline crustal thickness in the shelf is around 25 km with areas thinner than 20 km below the East Barents Basin, the Nordkapp and Sørkapp basins, and with areas thicker than 28 km beneath the Kong Karl Platform, Stappen High, Loppa High, Gardarbanken High, Sentralbanken High, Fedynisky High and the Central Barents High.

5.6 Top basement and Moho geometries compared with previous models

The model results presented here are compared with previous top basement and Moho depth compilations in Figs 10 and 11. Our modelled Moho depth is in quite good agreement with the Moho depth model of Grad *et al.* (2009); most of the differences are within ±2 km, and thus smaller than the uncertainties estimated for the Grad compilation (Fig. 10c). Larger differences are found in the Moho depth beneath the Vestbakken volcanic province, the Sørvestsnaget Basin and northern Bjørnøya, here our crust–mantle boundary is more than 8 km shallower (Figs 10c, 11b and c). Our

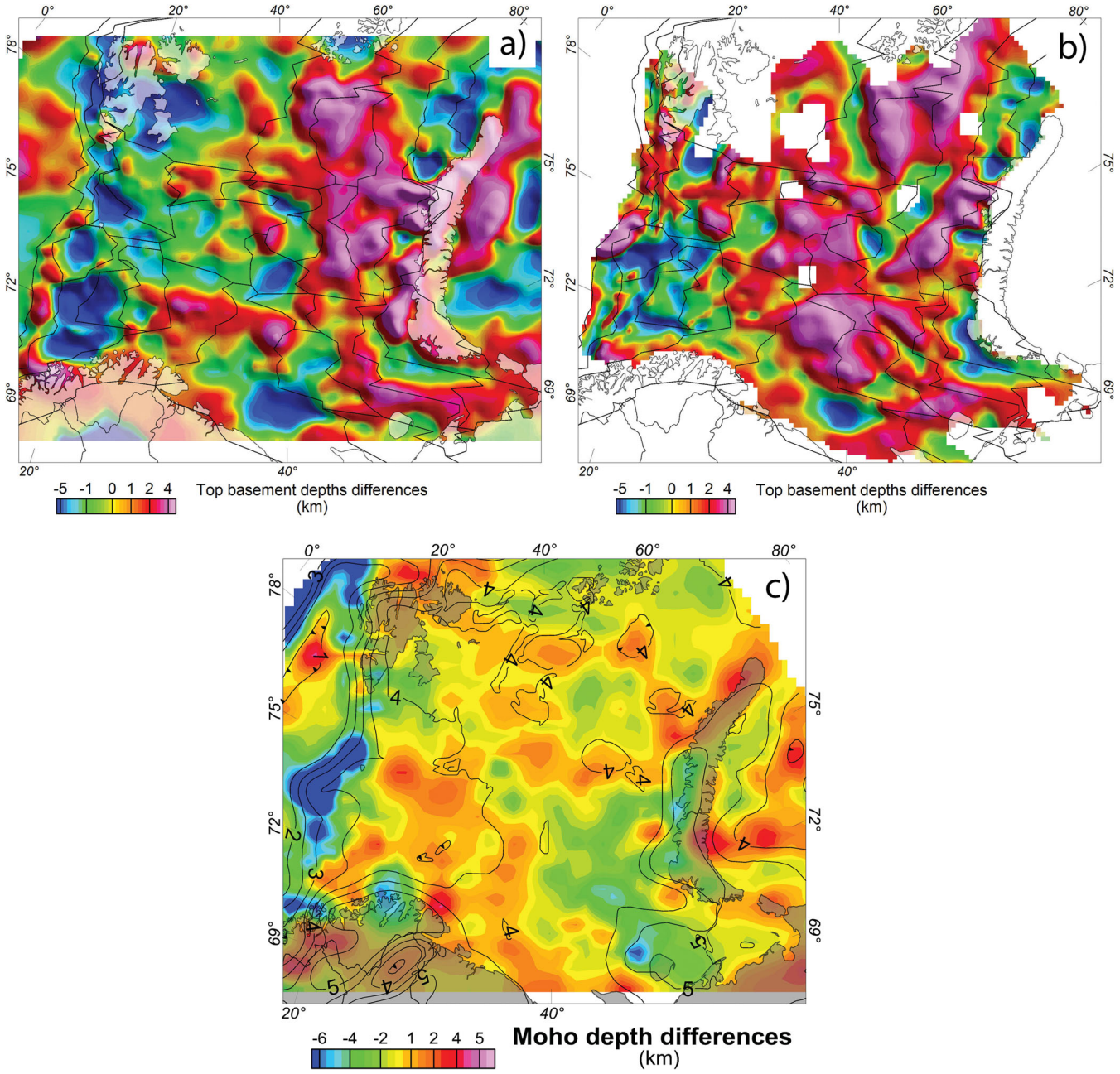

Figure 10. Top basement and Moho geometry results compared with existing models: (a) differences between our top basement (Fig. 7a) and Barents50 top basement (Ritzmann *et al.* 2007). (b) Differences between our top basement (Fig. 7a) and the Skilbrei (1990) basement for the West Barents Sea and Johansen *et al.* (1992) basement for the East Barents Sea. (c) Moho differences between our model results (Fig. 8b) and the Moho map of Grad *et al.* (2009). The contours show the uncertainty in the Moho map of Grad *et al.* 2009, in km.

new estimates are constrained by new geoplysical results (Clark *et al.* 2009; Marello *et al.* 2010), not included in the compilation by Grad *et al.* (2009).The top basement in the West Barents Sea is slightly shallower compared with previous models (Figs 10a and b and 11a and b), while in the East Barents Sea it is found to be about 4 km deeper (Figs 10a andb and 11b and c).

Some of the discrepancies may simply be a matter of basement definition and interpretation. The basement concept is not unique and depends on the target of the study and on the methodology. Three definitions of the top basement are commonly used: geological, magnetic and acoustic basement (e.g. Neuendorf *et al.* 2005; Sheriff 2006). Goussev & Pierce (2010) have emphasized the importance of clarifying the top basement definition properly in order to avoid misinterpretations and miscorrelations. It is important to note that the magnetic basement does not necessarily coincide with the real geological basement (e.g. if the basement is not magnetic). Also, the acoustic basement, which is commonly used as an upper constraint for the magnetic basement interpretation, can be structurally close to or coincident with the magnetic basement, or it can be much shallower (e.g. in the case of metasediments producing a velocity jump but not necessarily an increase in magnetization). If there is little velocity contrast between the lowermost sediments and basement, then the seismic basement itself is unlikely to be clearly defined and does not coincide with the magnetic basement.

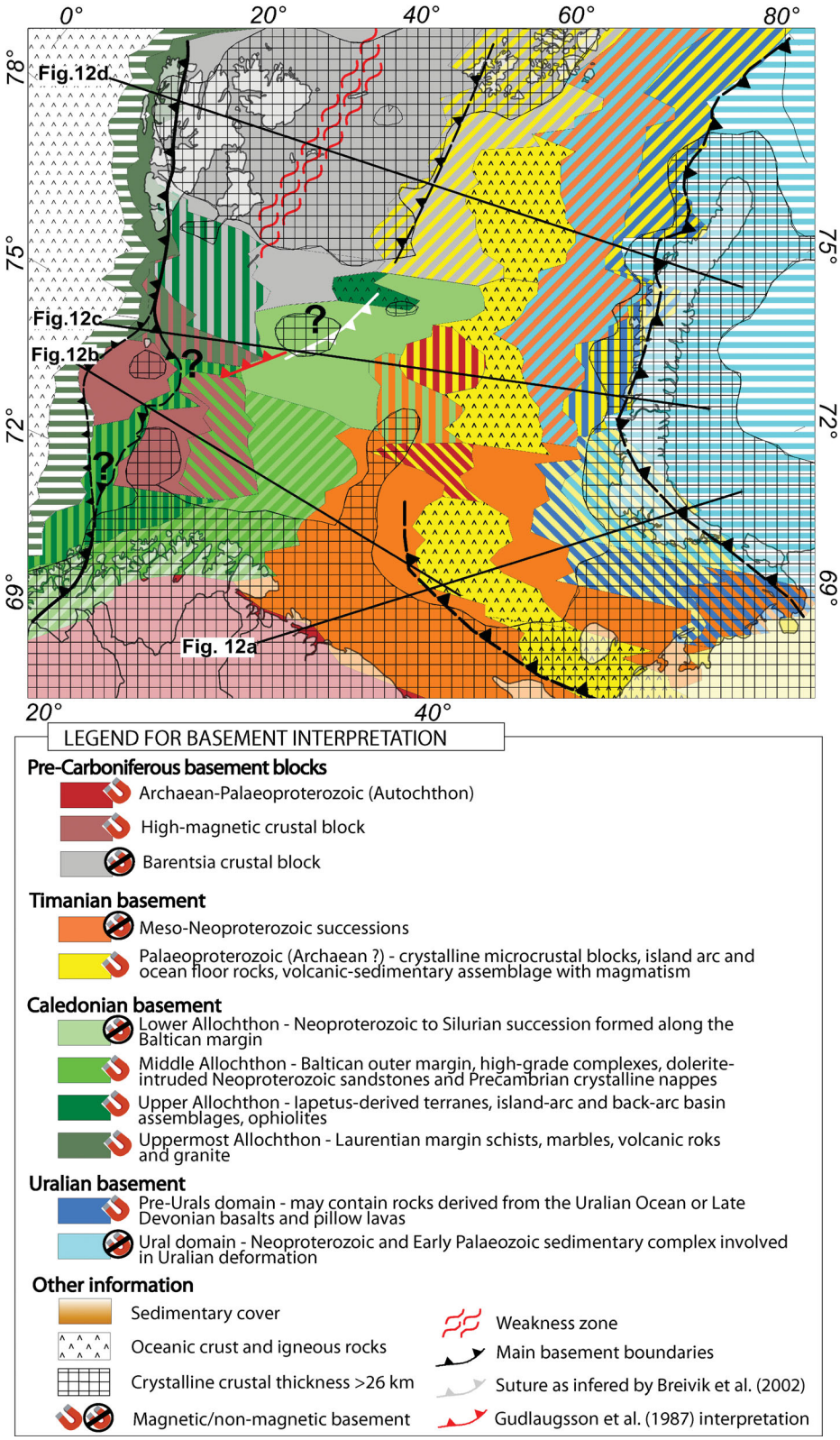

Figure 11. Basement interpretation map for the Barents Sea Region. The map shows the basement units defined in the 3D model organized into four major domains: pre-Carboniferous, Timanian, Caledonian and Uralian basement. The legend explains the different colours and patterns of the interpretation map and profiles (Fig. 11). Blocks with striped patterns represent the coexistence of two domains (e.g. Timanian basement reworked by Uralian Orogeny) or two different possible interpretations. The crystalline crustal thickness >26 km and the main basement boundary are also displayed. The four profiles are displayed in Fig. 11 and summarize the modelled basement properties and the finale interpretation.

In our model, we consider a basement, which approximates the real geological basement but, even so, ambiguity in this definition remains. The Riphean metasedimentary succession (Ectasian, Stenian and Tonian time in the International Commission on Stratigraphy), for example, has been seismically differentiated from the underlying crystalline upper crust and has been considered as part of the sedimentary package by Ivanova *et al.* (2006). In our model, we include the Meso-Neoproterozoic rocks as part of the basement, since they have been involved in the Timanian orogenic event and considered to be part of the Timanian basement terrane. Similarly, in the western Barents Sea, the pre-Devonian metasedimentary rocks that have been involved in Caledonian deformation are considered to be part of the Caledonian basement terrane. In general for the West Barents Sea, all pre-Carboniferous rocks have often been regarded as 'basement' rocks (Harland *et al.* 1997). On the other hand, in the East Barents Sea the Late Palaeozoic and Mesozoic sedimentary successions that may have been involved in Uralian orogenesis have not been included in what we define as the Ural basement terrane.

6 DISCUSSION

Our modelling approach allows us to identify basement units distinguished by densities and magnetic properties, and correlated with crustal geometries (top basement, Moho depth, crystalline crustal thickness), to propose a first-order geological interpretation of the Barents Sea crust, summarized in Figs 11 and 12.

The basement units have been organized into four major domains; pre-Carboniferous, Timanian, Caledonian and Uralian basement.

Pre-Carboniferous basement has been traced and divided into three major units. One corresponds to the Archaean–Palaeoproterozoic complexes exposed in the Fennoscandian Shield, a second unit forms isolated, high-magnetic, thick crustal blocks recognized beneath the Loppa High and Stappen High and a third unit constitutes the non-magnetic, thick crustal block that forms the Svalbard Platform.

The distinct magnetic properties of the low-magnetic Lower Allochthon, from the other, moderately magnetic Caledonian nappes and the high-magnetic Archaean–Palaeoproterozoic (Olesen *et al.* 2010; Barrère *et al.* 2011) allow us to interpret the basement in terms of Caledonian units. A prolongation of the different Caledonian nappes exposed in Finnmark into the southwestern Barents Sea has been proposed by several workers (Åm 1975; Olesen *et al.* 1990; Skilbrei 1995; Siedlecka & Roberts 1995; Barrère *et al.* 2011; Gernigon & Brönner 2012) and is reviewed here.

The Timanian terranes are distinguished by two units that represent a prolongation of the onshore geology: a high-magnetic domain which represents the aggregation of mafic and crystalline crustal blocks (island arcs, volcano–sedimentary assemblages and magmatic rocks), and a non-magnetic domain which characterizes the thick Meso-Neoproterozoic sedimentary successions (Fig. 12). The Timanian terranes are known to occur in the Southeast (Korago *et al.* 2004; Olovyanishnikov *et al.* 2000) and probably also in the Northeast Barents Sea.

The Uralian basement terrane is also subdivided into two units (Fig. 12). One corresponds to the continuation of the pre-Uralian domain (Kostyuchenko *et al.* 2006) that shows high-magnetic anomalies and may contain rocks of oceanic affinity. The other is composed of an agglomeration of non-magnetic units mostly comprising deformed Neoproterozoic and Early Palaeozoic complexes.

6.1 From the Archaean–Palaeoproterozoic fennoscandian shield to timanian

The Southeast Barents Sea is distinguished from the rest of the Barents Sea shelf by having higher density in the upper crust (Fig. 7a). The basement surface beneath Kola Peninsula and the Timan Ridge dips steeply towards the South Barents Basin and the Pechora Basin (Figs 1 and 6d). Moho depths vary from around 42 km in the onshore areas to 32 km under the South Barents Basin (Fig. 8b). In a previous study, Marello *et al.* (2010) supported the idea that the upper crust in the Southeast Barents Sea is most likely composed of Timanian complexes. Our crustal units are NW-SE oriented, like the Precambrian structures (Roberts & Siedlecka 2002), and have been interpreted as the prolongation of the onshore Pechora Basin Timanian terranes (Figs 1 and 8). The profile in Fig. 11a summarizes our model results and interpretation of the crustal geology in the Southeast Barents Sea.

The southwesternmost unit corresponds with the Archaean–Palaeoproterozoic crystalline basement which underlies large parts of the Fennoscandian Shield (Figs 11a and 12). It is characterized by medium–low densities, very high susceptibilities and an extremely thick continental crust. Such parameters have previously been associated with high-grade metamorphic rocks, including granulites (Barrère *et al.* 2010).

From the coast the basement changes to a low-magnetic and low-density domain (Fig. 11a). In this region, a thick Meso-Neoproterozoic mainly sedimentary succession (13 km in the Kola–Kanin Monocline) has been distinguished above the Archaean–Palaeoproterozoic basement (Verba & Sakoulina 2001; Ivanova *et al.* 2006). This sedimentary cover has been included in our model as part of the upper crust, a setup which resulted in a decrease of densities and magnetic properties of our crustal block. The unit corresponds to the offshore prolongation of the Meso-Neoproterozoic successions exposed in the Kanin and Rybachi–Sredni Peninsulas, which were deformed during the Timanian orogeny (Olovyanishnikov *et al.* 2000; Gee *et al.* 2006; Kostyuchenko *et al.* 2006).

Moving towards the South Barents Basin, the basement becomes highly magnetic and shows higher densities. This has been also interpreted as Timanian terranes consisting of deformed and transported island arc and ocean–floor magmatic assemblages with mafic to intermediate magmatism corresponding to a prolongation of the onshore Pechora Zone (Gee *et al.* 2006; Fig. 12) Alternatively, it could represents an agglomeration of small microcontinental blocks and slivers (Getsen 1991) intruded by magmatic plutons of variable character and chemistry, and metamorphosed in amphibolite facies corresponding to the onshore Khoreyver Domain (Beliakov & Stepanenko 1991; Kostyuchenko *et al.* 2006).

Beneath the central part of the South Barents Basin we see a dense and low-magnetic crust (Fig 11a). The low-magnetic properties are proposed to be the result of the Timanian terranes accretion reflecting a non-magnetic Meso-Neoproterozoic succession lying above magnetic crystalline metamorphic or magmatic rocks similar to those of the western units (Figs 11a and 12). This scenario is similar to the one found in northwestern Kola Peninsula, where the gravity and magnetic signal of the crystalline basement is blurred by the Meso-Neoproterozoic sedimentary cover which was partly overthrust during the Timanian orogeny. Compared to the weakly deformed Riphean rocks found in the Fedynskiy High area (Ivanova *et al.* 2006), we think that under the South Barents Basin, the Riphean (Meso-Neoproterozoic) succession was first strongly deformed during the Timanian orogeny and later buried under a thick

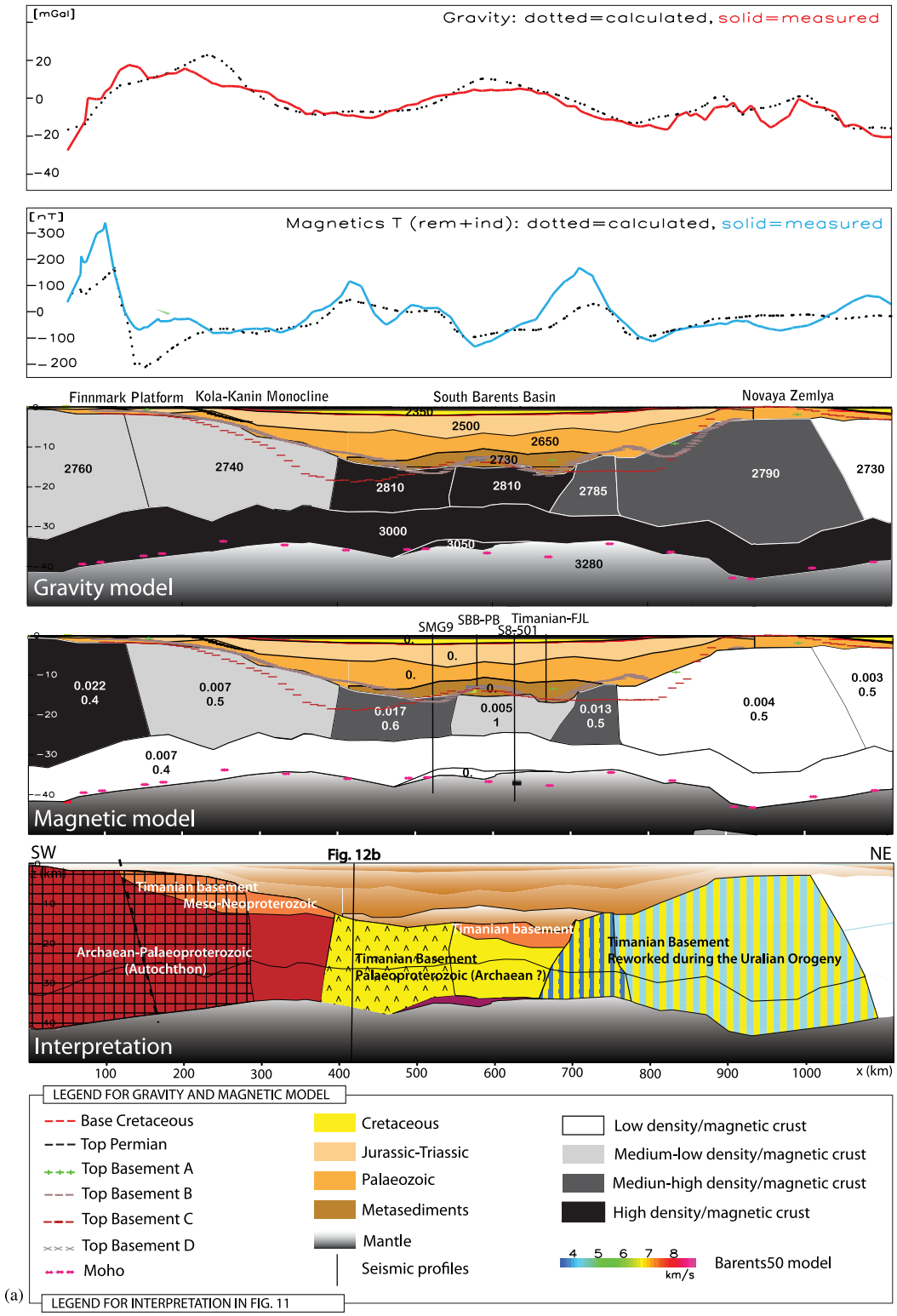

Figure 12. Four profiles displaying the model results and the final interpretation: (a) Southeast Barents Sea; (b) Southwest Barents Sea; (c) the Central west and Central east Barents Sea; and (d) the North Barents Sea (see Fig. 11 for locations). The two upper panels show respectively the gravity and magnetic field, calculated and observed. In the three lower panels, the gravity model with the geographical locations (see Fig. 1 for geographical locations) is displayed. The numbers in the model indicate the densities in kg m^{-3}. The underlying panel shows the magnetic model; the two numbers in the crust indicate the susceptibility (SI) and the Q (Königsberger) ratio. The names on top of the 2D crossing seismic line are plotted (for locations see also Fig. 2). The lowest panel shows the interpretation of the model (for the legend, see Fig. 11). In Fig. 11a, the legend for the additional information is displayed for all the four transects. The top basement models are: top basement A (Barents50, Ritzmann *et al.* 2007); top basement B (Skilbrei 1991 for the West Barents Sea, Johansen *et al.* 1992 for the East Barents Sea); top basement C (Gramberg *et al.* 2001); top basement D (Barrère *et al.* 2010). The Moho plotted is from Grad *et al.* (2009). The sediment boundaries were provided by Statoil (see Table 3).

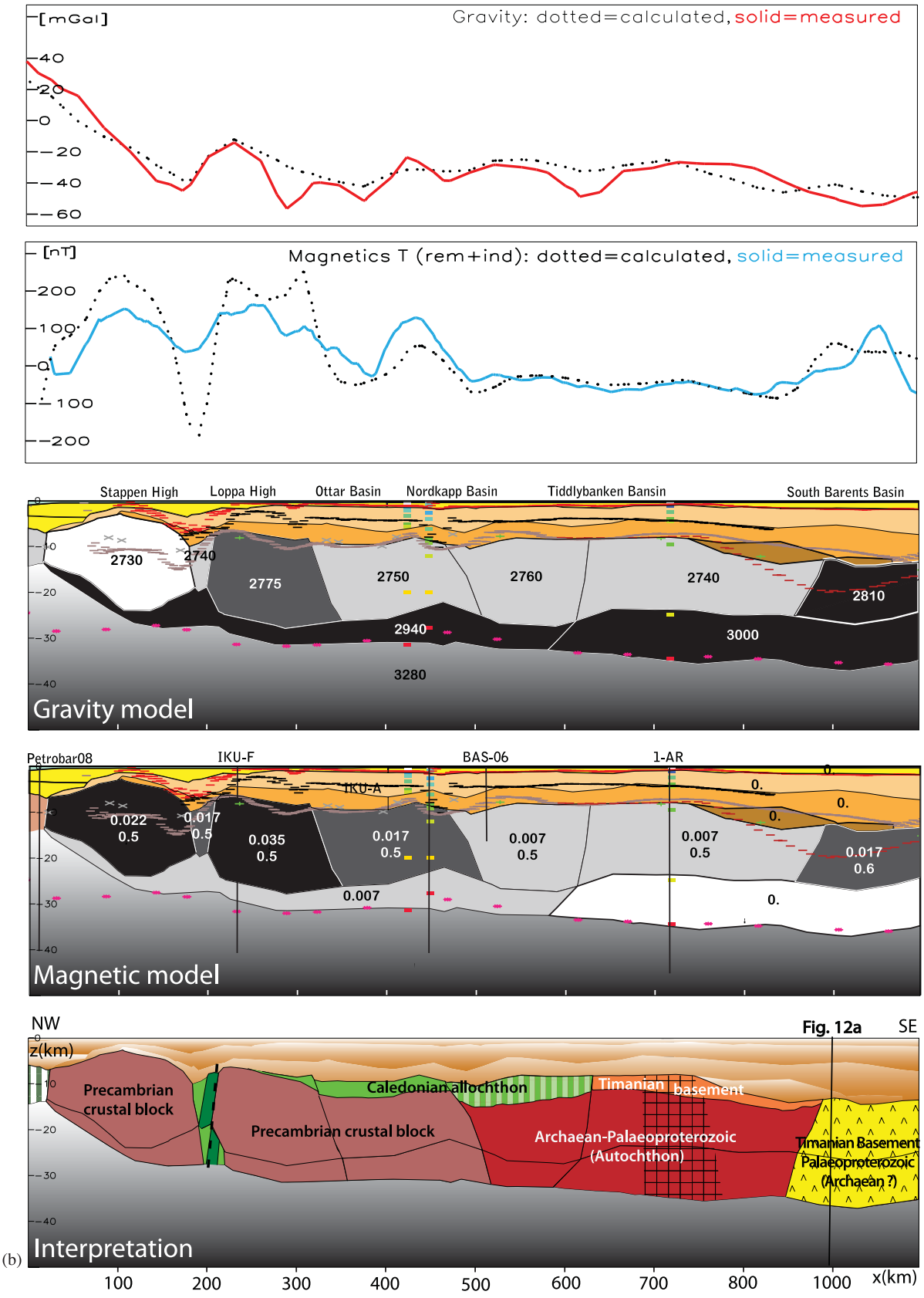

(b)

Figure 12 – *(continued.)*

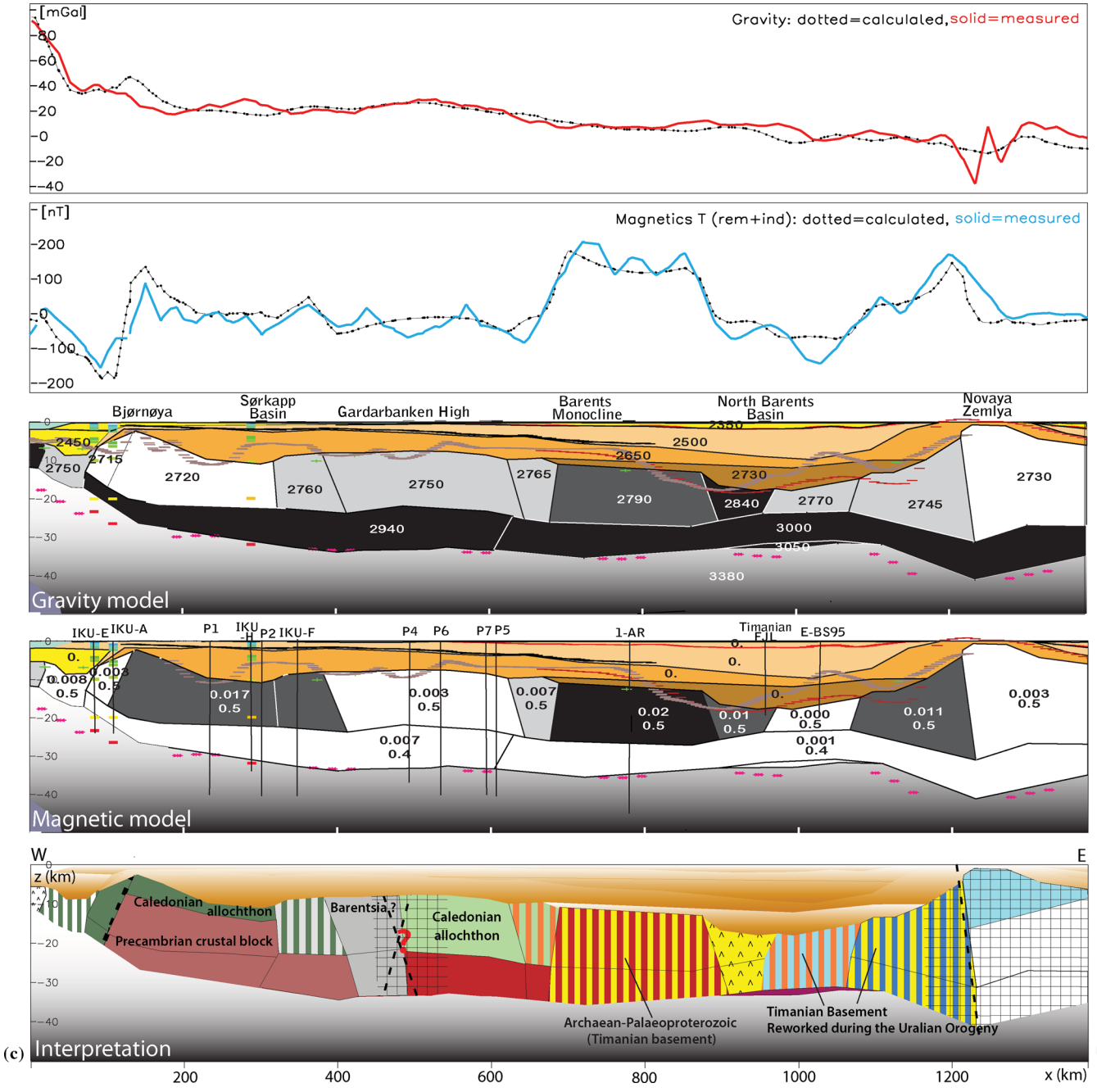

Figure 12 – *(continued.)*

sedimentary cover (more than 15 km). This led to a metamorphism of the older Precambrian successions resulting in a significant increase of densities.

Farther east, the eastern flank of the South Barents Basin has a medium–high magnetic and medium–high dense crust (Figs 11a and 12) and is interpreted to be the continuation of the pre-Urals Domain defined by Kostyuchenko *et al.* (2006). It consists of a Precambrian crust that contains rocks of oceanic affinity. Alternatively this unit could be interpreted as the extension of the Bolshezemel block as has been already described by Kuznetsov (2007) including volcano–sedimentary rocks, felsic volcanics and intrusions of two-mica granites and gabbros. Most of the south island of Novaya Zemlya differs from the central and northern parts (Fig. 12). The Timanian orogeny is known to have affected this southern area (Pease & Scott 2009), as proposed from the analysis of outcopping Precambrian rocks (Korago *et al.* 2004) and from a study of the magnetic trends (Marello *et al.* 2010). The Late Permian–Triassic Uralian deformation reactivated the pre-existing Timanian terranes. The telescoped thrusted terranes could partly explain the thickening of the crust (Fig. 11a) and the formation of a wedge composed of Neoproterozoic and Late Palaeozoic metasedimentary units (Korago *et al.* 2004; Stoupakova *et al.* 2011) corresponding to low-magnetic units. This wedge of sedimentary assemblages overthrusts older high-magnetic basement (maybe Archaean–Palaeoproterozoic) similar to the crystalline basement below the Timan–Pechora Basin region (Figs 11a and 12).

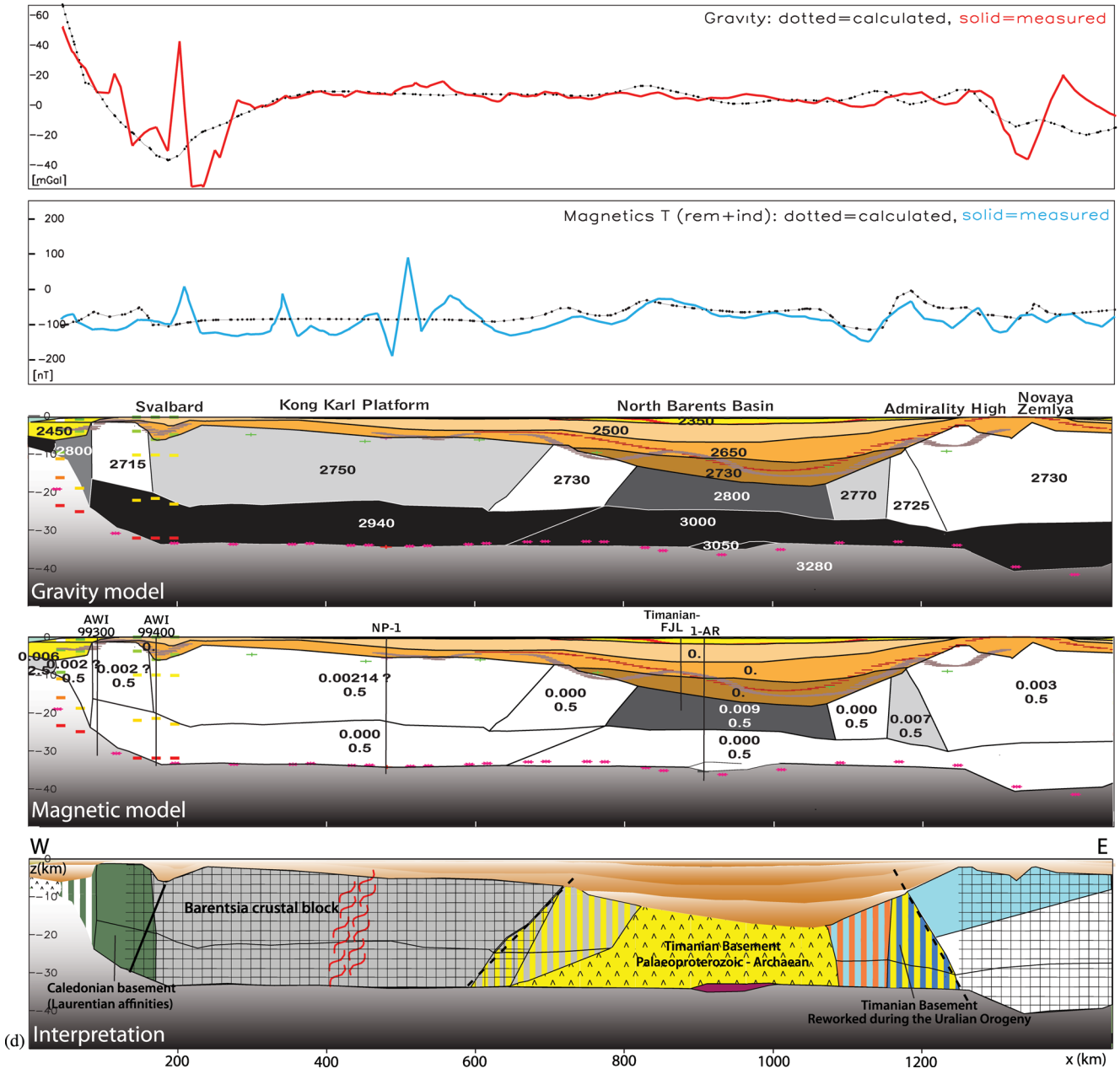

(d)

Figure 12 – *(continued.)*

6.2 Southwest Barents Sea: from Caledonian to Timanian

The Southwest Barents Sea has medium- to high-magnetic upper basement units (Fig. 7) that correlate with the main structural elements (Gabrielsen *et al.* 1990) on top of a magnetic lower crust (Fig. 11b). In the West Barents Sea, the transition from the oceanic to the continental domain is characterized by a basinal province that originated during Late Mesozoic extension, which runs more or less parallel to the Senja Fracture Zone (SJZ in Fig. 1). In our model, the margin is defined by a basement block that extends under part of the Harstad and Sørvestsnaget Basins and ends at the Vestbakken volcanic province (Figs 1 and 12) and is characterized by an extremely thinned, stretched crust (Fig. 11b). This unit has been interpreted as transitional crust of intermediate character between continental and oceanic crust.

The transect cuts two crustal blocks characterized by extremely high-magnetic crust, and by a crustal thickness thicker than the average shelf thickness and shallower top basement (Fig. 11b). These units correspond with the Loppa High and the Stappen High, and are interpreted as micro-blocks of a different basement type compared to their surroundings (Figs 11b and 12). The Loppa High basement is penetrated by wells and results reveal the presence of amphibolites with a significantly high magnetization, which are possibly related either to the Seiland Igneous Province or to nappes in the Uppermost Allochthon (Slagstad *et al.* 2008). More recent information stems from seismic models that record anomalous high velocities in the mantle below the Loppa High, similar to the upper mantle

velocities estimated for the Varanger Peninsula (Clark *et al.* 2009). This observation leads us to interpret the main crust of the Loppa High at being composed of high-grade metamorphic rocks, possibly granulites, similar to parts of the Archaean–Palaeoproterozoic basement in the Fennoscandian Shield, and with a thin cover of allochthonous terranes (Upper or Uppermost Allochthon) (Figs 11b and 12). Similarly, the Stappen High is believed to be composed of comparable high-grade metamorphic rocks but its relationship to the Archaean–Palaeoproterozoic basement is doubtful. The crystalline crust of the Stappen High could be a basement block with Laurentian affinities (Breivik *et al.* 2005), or an independent microcrustal block initially located between Laurentia and Baltica and subsequently involved in the Caledonian orogeny. Alternatively, Olesen *et al.* (2010) from interpretation of the magnetic anomalies associated the two units as the northward continuation of the TIB (Transscandinavian Igneous Belt).

Located between the two magnetic basement blocks, a thin crustal unit extends below the Bjørnøya Basin, Tromsø Basin and Hammerfest Basin. In the deepest part of the Bjørnøya Basin (which has a 12-km thick sedimentary succession) the upper crust gets thinner and a high-density and magnetic lower crust and Moho are rising up in this area (Fig. 11b). Our crustal geometry is in agreement with new refraction data (Clark *et al.* 2009) and could be an example of exhumation of a lower crust that developed during the Late Mesozoic thinning phase of the western Barents Sea, as already proposed by Barrère *et al.* (2009). More local studies (Clark *et al.* 2009; Barrère *et al.* 2011) also presented a different scenario, proposing the existence of a high-density lower crustal body under the Bjørnøya Basin and part of the Loppa High. The quite high susceptibility of the crust could be explained by the presence of magnetic gneisses comparable to the ones mapped and sampled onshore Norway (Olesen *et al.* 1990, 2010; Barrère *et al.* 2011), and with the medium-grade complexes, dolerite-intruded Neoproterozoic sandstones and Precambrian crystalline nappes that form most of the Middle Allochthon. An alternative explanation could involve ophiolites, island arc and backarc basin assemblages that occur in the Upper Allochthon in many parts of Norway (e.g. Furnes *et al.* 1985; Gee *et al.* 2008; Figs 11b and 12).

Moving southeast of the Loppa High, a crustal block extends from the southern part of the Nordkapp Basin, below the Ottar Basin and part of the Bjarmeland Platform (Figs 11 and 12). Previous studies recognize a lateral deflection of the Caledonian structures at this location (Gernigon *et al.* 2007; Barrère *et al.* 2009; Gernigon & Brönner 2012). This corresponds to medium- to high-grade metamorphic Caledonian rocks that are part of the Middle and Upper Allochthons lying on top of the crystalline crust. The crust beneath is interpreted to be similar to the Archaean–Palaeoproterozoic crust forming the Fennoscandian Shield or the Loppa High (Figs 11b and 12).

Beneath the Nordkapp Basin, another basement unit has been defined (Fig. 11b). It extends from the coastal zone of northern Norway mostly parallel to the Troms–Finnmark Fault Complex (TFFC) and the Måsøy Fault Complex (MFC) to the Bjarmeland Platform (Figs 1 and 12). Similar to the western unit the petrophysical properties suggest that the crust could correspond to the extension of the basement unit defined by Barrère *et al.* (2011) and interpreted as Caledonian terrane including the Lower and Middle allochthons (dominated by lower densities and magnetic properties) overlying the older Archaean–Palaeoproterozoic crust (Figs 11b and 12). Farther to the southeast, the transect leaves the Caledonian domain and crosses into the Timanian basement units described in the previous section.

6.3 Transition between north and south Barents Sea

The central–west Barents Sea represents a transitional region from the southern high-magnetic crust dominated by structural basement highs and lows to the northern platform area characterized by non-magnetic crust (Figs 7 and 12). The transition between these northern and southern areas of the Barents Sea is summarized in Fig. 11c.

From the western margin, the transect passes across a basement block that extends northeast of the Stappen High including a large part of Bjørnøya and the northeasten areas of the Barents Sea (Figs 11c and 13). Pre-Ordovician dolomites, sandstones, shales and limestones exposed in the south of Bjørnøya are interpreted as basement with a northeastern Greenland affinity (Smith 2000). Our model suggests a top basement geometry that links the Stappen High with Bjørnøya (Fig. 6d). This observation, combined with the petrophysical parameters applied in the model (lower densities and lower magnetic properties compared to the Stappen High), leads to the interpretation that Bjørnøya is made up of two different basement types: a crystalline crust related to the Stappen High crustal block, and a cover of Caledonian nappes. During the Caledonian collision Late Neoproterozoic to Ordovician terranes with Laurentian affinities (Holtedahl 1920; Dallmann & Krasil'ščikov 1996; Smith & Rasmussen 2008) were thrusted above the deeper Precambrian crustal block, generating the complex that is exposed on Bjørnøya today. We correlate this Caledonian thrust cover with the Uppermost Allochthon unit of mainland Norway (Figs 11c and 12).

Farther east, the transect crosses a basement unit that extends northward beneath the Sørkapp Basin and Edgeøya Platform (Fig. 12). The crustal geometry (Figs 6d, 8 and 9) and petrophysical values applied suggest a transition from a crustal type composed of magnetic terranes, similar to those found in the Southwest Barents Sea, to a thick and non-magnetic crystalline crust as exposed in the Svalbard region (Fig. 12). Seismic records indicate an increase in *P*-velocity and V_P/V_S ratio in the crust northeastwards from the margin north of Bjørnøya, suggesting an increase in density and a more mafic rock composition (Breivik *et al.* 2003, 2005). This mafic composition and density increase could be explained as a transition from the Uppermost Allochthon, comprising shelf and slope-rise successions (Roberts 2007; Gee *et al.* 2008), to the diverse Iapetus Ocean terranes of the Upper Allochthon (Figs 11c and 12).

Under the Gardarbanken High (Figs 1 and 11c), the basement becomes non-magnetic and is thickening, correlating with a shallowing of the basement and a slight deepening of the Moho. Here, Breivik *et al.* (2002) proposed an interpretation involving a deep, eclogitized, crustal root associated with an inferred old Caledonian suture (see Fig. 12). We interpret the crust in the north of Gardarbanken to be composed of low-magnetic rocks that have affinities with the Svalbard block. On the other hand, the basement in the south is interpreted to be mostly composed of terranes linked with the Baltican platform and margin, which are now part of the Lower Allochthon (Figs 11c and 12).

A sag basin with a sediment record that spans from the late Palaeozoic to the Mesozoic is present in the East Barents Sea. The lithology of the basement beneath the sedimentary succession is difficult to interpret due to the sparsity of data that reach the crust. The geometry of our modelled crustal unit reflects the arc-shaped geometry of the Novaya Zemlya Fold Belt observed farther to the east and may be related similarly to Novaya Zemlya with pre-Uralian structures (e.g. Scott *et al.* 2010).

The western flank of the basin is underlain by a high-magnetic basement. Two prominent magnetic units (susceptibility >0.2 SI)

are distinguished from the rest of the crust and produce the two central Barents Sea magnetic anomalies (Fig. 3b). Both structures are corresponding with shallow Archaean–Palaeoproterozic basement but are not imaged as a different type of crust on crossing seismic-reflection data (1-AR profile, Ivanova *et al.* 2006). Our model suggests distinct properties for these two units compared with the surrounding crust (Figs 7 and 11c). The shallow Archaean–Palaeoproterozoic basement could imply a thinning or total removal of the Neoproterozoic non-magnetic cover, which is included in the basement layer defined in our model. This results in crustal units with a higher average magnetization entirely made up of granulite rocks. Another possible explanation is a relationship with mafic magmatic bodies, which could be part of older Timanian terranes observed beneath the Pechora Zone (Dovzhikova *et al.* 2004).

The eastern basement unit crossed by the transect still forms the western flank of the basin (Figs 11c and 12). We explain this unit as a complex of island arc, ocean-floor magmatic rock or volcano–sedimentary assemblage with mafic to intermediate magmatism considered to be the prolongation of the Pechora Zone described by Gee *et al.* (2006). This interpretation is based on the idea that the Timanian range extends farther north mimicking the arcuate shape of Novaya Zemlya. An alternative interpretation is that the crust is of oceanic origin. Aplonov *et al.* (1996) have argued that in the Devonian, during a pre-Uralian rifting phase, oceanic crust was generated and formed a precursor basin to the East Barents Basin. The higher densities are explained by sedimentary compaction and the gabbroic and basaltic rock compositions of the proposed oceanic domain.

Farther east buried under the East Barents Basin, an almost non-magnetic and low-density unit has been defined (Figs 11c and 12). Its petrophysical properties are explained by an aggregation of Precambrian terranes most likely related to Neoproterozoic sedimentary successions that may be affected by Timanian and later by Uralian deformation. We suggest that the Uralian deformation ends in the proximity to this crustal block (Figs 11c and 12).

West of Novaya Zemlya, the crustal geometry is variable but thinning is recognized towards the centre of the basin (Figs 6c, 8 and 11c). The crust forming the eastern flank of the South and North Barents Basins is steep compared to the western flank of the basin. This geometry is an indication of the multiphase evolution of the basin that evolved at one stage as a foreland basin (e.g. Gramberg 1988; Ziegler 1989; Petrov *et al.* 2008). The intermediate magnetic properties and low densities characterizing this crust lead us to propose this unit as being part of the pre-Uralian domain as defined by Kostyuchenko *et al.* (2006). It may represent a crust that is Precambrian and may contain rocks of oceanic affinity obducted during the Uralian orogeny or accreted towards Baltica during the Timanian (Fig. 12).

The eastern unit encountered along the profile (Fig. 11c) is the analogue to the one described in the transect Fig. 11a in the south Novaya Zemlya region, with the difference that no Timanian deformation has been proposed for this area (Korago *et al.* 2004).

6.4 Northern Barents Sea: from Svalbard to the North Barents Basin

The transect displayed in Fig. 11d shows the setting of the northern Barents Sea. The Northwest Barents Sea is mainly a platform area where Mesozoic tectonism produced smaller structures (Grogan *et al.* 1998) compared to the Southwest Barents Sea. One of the reasons for differentiating the Northwest from the Southwest Barents Sea is the different evolution of the margin north of the Stappen High compared to the south (Faleide *et al.* 2008). Moreover, the inherited Caledonian structures (Ziegler 1988; Doré 1991) and pre-Caledonian geology identified here play an important role.

The transect (Fig. 11d) shows a crustal unit in the west that extends along the Hornsund Fault Zone (HFZ) and Sørkapp Fault Zone (SKZ) (Fig. 1), and corresponds with a complex sheared and rifted margin (Faleide *et al.* 2008). In the northwest of Spitsbergen the continental crust thins rapidly towards the Svalbard margin (Fig. 11c). In the same way as for the southern margin (Fig. 11b), the unit has been interpreted as crust with an intermediate character between continental and oceanic crust. This might have been produced by the interaction of the continental crust with the mantle during extension and break up (Fig. 12).

The western unit (Figs 11c and 12) includes the western part of Svalbard with exposed basement comprising an amalgamation of different terranes (Late Mesoproterozoic, Early Neoproterozoic) that differs from the rest of Svalbard. The onshore unit has an affinity with the Pearya terrane of northernmost Ellesmere Island in northern Canada and with Laurentia (Harland *et al.* 1997; Trettin 1998; Gee & Teben'kov 2004).

The eastern and central Svalbard unit differs from the west for two main reasons: (1) the low-magnetic crust (Fig. 11d) and (2) the crustal geometry characterized by a shallow basement and thick crust (Figs 6d, 9a and 11d). An explanation for the low-magnetic crust is not easy to deduce. Pseudo-gravity transformation, which enhances the effect of large and deeper structures, indicates low-magnetic properties for the region (Marello *et al.* 2010). In Nordaustlandet (Northeast Svalbard), there are Neoproterozoic volcanic rocks, granites and migmatites, which thus make it difficult to explain such a low-magnetic crust. The different polarity of paleomagnetic field directions and the remanence of magmatic intrusions may be an explanation, but the modelling of remanent magnetization was not sufficient to explain the magnetic anomaly. Moreover, the presence of large Early Cretaceous intrusions east of Svalbard (Grogan *et al.* 1998) correlates with the high-frequency magnetic pattern observed in the area. The presence of this young and shallow magmatism affects the magnetic signal and precludes the analysis of deeper and larger basement magnetic sources. The distribution of these intrusions has been interpreted to relate to an old basement weakness zone of Caledonian origin (Barrére *et al.* 2010). Besides these modelling difficulties, our results provide an indication of the existence of a thick crustal block characterized by very different and distinct magnetic properties. This may suggest a different origin for the central and eastern Svalbard block and could be related to the—concept of a Barentsia micro-crustal block (Figs 11c and 12) as earlier suggested by Gudlaugsson *et al.* (1998), but intended here as an independent fragment which does not correspond to the archipelago of Svalbard as it presently exists. The transition from the Svalbard block to the North Barents Basin is marked by a low-density and poorly magnetic basement unit (Figs 11c and 12). This unit extends from southwest of Franz Josef Land and links the proposed Svalbard Craton (Barentsia) with the North Barents Basin. The basement consists of Neoproterozoic rocks similar to those found in the Franz Josef Land (Dibner 1998). Its thickness diminishes towards the North Barents Basin and this geometry could be the result of the initial rifting (probably Late Devonian) that caused the crustal thinning and the formation of the early North Barents Basin.

Farther east, the profile displays the North Barents Basin, which is dominated by a basement that represents the

continuation of the domains described in the previous section (Figs 11c and 12).

6.5 Caledonian–Timanian extension and interaction

The offshore extension of the Caledonian and the location of one 'branch-suture zone' or 'bifurcate-suture zone' separating Baltica and Laurentia terranes has been matter of extensive discussion (e.g. Harland & Gayer 1972; Siedlecka 1975; Gudlaugsson *et al.* 1987, 1998; Ziegler 1988; Doré 1991; Johansen *et al.* 1994; Nikishin *et al.* 1996; Fichler *et al.* 1997, Breivik *et al.* 2002; Gee *et al.* 2006; Ritzmann *et al.* 2007; Barrère *et al.* 2011; Pease 2011; Gernigon & Brönner 2012). While we support the idea of the existence of two Caledonian branches (Siedlecka 1975; Gudlaugsson *et al.* 1998), we propose a different location than in previous studies.

One branch corresponds to the site of the Laurentia–Baltica collision and extends northwards from northern Norway, passing to the west of the Loppa High and also probably west of the Stappen High, and continuing to the east of the southwestern Svalbard terrane as defined by Gee *et al.* (2008). This location mostly coincides with the extension of the here interpreted Upper Allochthon terranes (Fig. 12).

A second Caledonian branch occupies the Northwest Barents Sea. We support the idea that a microcrustal block (Barentsia), including the actual central eastern Svalbard and Svalbard platform, was involved in the Caledonian orogeny (e.g. Pettersson *et al.* 2009 and references therein) and that the boundary between Baltica and Barentsia has to be in the central part of the Barents Sea. Barrère *et al.* (2009) proposed the existence of a more competent terrane to the north of Baltica to justify the contrasting tectonic setting between the northern and the southern Barents Sea and to create their proposed elbow-shape in the offshore extension of the Caledonian thrusts. We validate the existence of this competent block, suggesting it to be a thick crustal body distinct from the other crustal units, which we relate with Barentsia.

Ocean bottom seismic data denote the existence of a SE-dipping, inferred Caledonian suture extending beneath a 'deep crustal root' located in proximity to the Gardarbanken and Sentralbanken highs and Olga Basin (Fig. 12, Breivik *et al.* 2002). We agree with the possible location of the suture between Barentsia and Baltica in this area and extend this boundary north–northeastwards to the western part of Franz Josef Land.

The orientation of this inferred suture can be discussed. The profiles displayed in Fig. 11d show boundaries between the Svalbard crustal block and the eastern units which dip at depth toward the northwest. We can assume that these reflect the orientation and dip of the major thrusts and a link to the westward-dipping reflectivity interpreted as an eastward overthrust by Gudlaugsson *et al.* (1987) (Fig. 12). On the contrary, in proximity to the Gardarbanken High (Fig. 11c) the crustal boundaries dip towards the southeast and simulate the major thrust geometry interpreted as a suture by Breivik *et al.* (2002).

The observed increase in thickness of the crystalline basement, which coincides with the Fedynskiy and Central Barents highs (Figs 10b, 11b and 12) could support the idea that the Fedynskiy and Central Barents highs are microcontinental blocks (Aplonov *et al.* 1996). A proper understanding of their existence and formation is important since these two blocks are located roughly at the Caledonian and Timanian deformation fronts. On Varanger Peninsula, the Caledonian structures are dying out eastwards and, conversely, the Timanian structures gradually decrease westwards (Roberts & Olovyanishnikov 2004; Herrevold *et al.* 2009). That situation could be extended offshore where the Caledonian nappes that swing around the Loppa High (Barrère *et al.* 2009, 2011; Gernigon & Brönner 2012) are separated by the Fedynskiy and Central Barents Highs from the Timanian terranes which swing in the opposite sense in an arc shape that mimics the geometry of Novaya Zemlya. The observation made by Scott *et al.* 2010 to explain the bended shape of Novaya Zemlya, furnish an argument to support our interpretation that the arcuate shape of the basement units under the eastern Barents Sea is a geometry that reflects the Timanian accretion of different crustal units and is not related to a Permo–Triassic, Uralian event.

7 CONCLUSIONS

We have developed a new model for the Barents Sea that integrates potential field modelling with pre-existing models. Our modelling refines the crustal architecture and provides density and magnetic distributions for the entire region. The final result improves our understanding of the Barents Sea geology in space and time.

Three major regions are distinguished in our model; (1) the Southwest Barents Sea, (2) the Northwest Barents Sea and (3) the eastern Barents Sea. Large differences between these areas are recognized in terms of top basement geometry, crustal thickness and crustal properties, which reflect their different tectonic histories.

Comparative observations of our crustal setting and properties results with previous models, allow us to propose a new interpretation for the basement beneath the Barents Sea.

(1) The Southwest Barents Sea crust is of high-magnetic character and is composed of Precambrian basement mostly covered by Caledonian terranes. The Caledonian units occurring along the Baltica–Laurentia margin correspond to aggregation series of nappes characterized by medium-magnetic (except for the Lower Allochthon which is non-magnetic) overlying older basement terranes (Fennoscandian Shield, Loppa High and Stappen High).

(2) The Caledonian basement in the Northwest Barents Sea comprises terranes formed at the margin between the Svalbard Craton (Barentsia) and Laurentia, and is dominated by medium-low densities and a non-magnetic basement. The central Barents Sea in proximity to the Sentralbanken High is distinguished from the Southwest Barents Sea by its low-magnetic properties. It is composed of crustal terranes developed between the platform margin of Baltica and the Barentsia margin, which were thrust together during the Caledonian event. The existence of a second branch of Caledonian basement in this area is supported by our model.

(3) The basement beneath the North Barents Basin is dominated on its western flank by high-magnetic and high-density crust interpreted as Precambrian basement, which may have been affected by Timanian deformation. The central part of the basin is underlain by a non-magnetic and less dense crust, including Meso-Neoproterozoic or younger successions lying close to the Uralian front. The steeper eastern flank with higher magnetic and less dense crust is considered to have oceanic or magmatic affinities and to have been strongly affected by the Uralian deformation.

(4) The crust of the Southeast Barents Sea represents an extension of the Timan–Pechora basement domains. This region is characterized by a high-density basement and by an alternation of high-magnetic and non-magnetic blocks. The non-magnetic crust is considered to represent the Meso-Neoproterozoic successions on top of older, magnetic, crystalline crust.

ACKNOWLEDGEMENTS

The study was carried out as part of the PETROBAR project (Petroleum-related regional studies of the Barents Sea region) funded by Statoil and the PETROMAKS programme of the Research Council of Norway. We thank Odleiv Olesen, Marco Brönner and Christine Fichler for sharing their knowledge about the Barents Sea. We are very grateful to David Roberts for editorial review before manuscript submission. The authors thank V. Pease and G.S. Kimbell for their constructive critics and comments, which improved the quality of the manuscript.

REFERENCES

Åm, K., 1975. Aeromagnetic basement complex mapping north of latitude 62N. Norway, *Norges Geologiske Undersøkelse,* **316,** 351–374.

Aplonov, S.V., Shmelev, G.B. & Krasnov, D.K., 1996. Geodynamics of the Barents-Kara shelf: geophysical evidence, *Geotectonics,* **30**(4), 309–326.

Athy, L.F., 1930. Density, porosity, and compaction of sedimentary rocks, *AAPG Bull.,* **14,** 1–24.

Barrère, C., Ebbing, J. & Gernigon, L., 2009. Offshore prolongation of Caledonian structures and basement charaterisation in the western Barents Sea from geophysical modelling, *Tectonophysics,* **470**(1–2), 71–88.

Barrère, C., Ebbing, J. & Gernigon, L., 2011. 3D density and magnetic crustal characterisation of the southwestern Barents Shelf: implications for the offshore prolongation of the Norwegian Caledonides, *Geophys. J. Int.,* **184,** 1147–1166.

Beliakov, T. & Stepanenko, I., 1991. Magmatism and geodynamics of the Baikalide basement of the Timan-Pechora syneclise, *Izvestiya Akademii Nauk SSSR, Seriya Geologicheskaya* [in Russian], **12,** 106–117.

Birch, F., 1961. The velocity of compressional waves in rocks to 10 kilobars, Part 2, *Geophys. Res.,* **66**(7), 2199–2224.

Blakely, R.J., 1996. *Potential Theory in Gravity and Magnetic Applications,* Cambridge University Press, Cambridge, 441 pp.

Bonatti, E. & Michael, J.P., 1989. Mantle peridotites from continental rifts to oceanic basins to subduction zones, *Earth planet. Sci. Lett.,* **91,** 297–311.

Breivik, A.J., Gudlaugsson, S.T. & Faleide, J.I., 1995. Ottar-Basin, SW Barents Sea: a Major Upper Palaeozoic rift basin containing large volumes of deeply buried salts, *Basin Res.,* **7**(4), 299–312.

Breivik, A.J., Faleide, J.I. & Gudlaugsson, S.T., 1998. Southwestern Barents Sea margin: Late Mesozoic sedimentary basins and crustal extension, *Tectonophysics,* **293,** 21–44.

Breivik, A.J., Verhoef, J. & Faleide, J.I., 1999. Effect of thermal contrasts on gravity modeling at passive margins: Results from the western Barents Sea, *J. geophys. Res.-Solid Earth,* **104**(B7), 15 293–15 311.

Breivik, A.J., Mjelde, R., Gorgan, P., Shimamura, H., Murai, Y., Nishimura, Y. & Kuwano, A., 2002. A possible Caledonide arm through the Barents Sea imaged by OBS data, *Tectonophysics,* **355,** 67–97.

Breivik, A.J., Mjelde, R., Grogan, P., Shimamura, H., Murai, Y. & Nishimura, Y., 2003. Crustal structure and transform margin development south of Svalbard based on ocean bottom seismometer data, *Tectonophysics,* **369**(1–2), 37–70.

Breivik, A.J., Mjelde, R., Grogan, P., Shimamura, H., Murai, Y. & Nishimura, Y., 2005. Caledonide development offshore–onshore Svalbard based on ocean bottom seismometer, conventional seismic, and potential field data, *Tectonophysics,* **410,** 79–117.

Carlson, R.L. & Herrick, C.N., 1990. Densities and porosities in the oceanic-crust and their variations with depth and age, *J. geophys. Res.-Solid Earth Planets,* **95**(B6), 9153–9170.

Christensen, N.I. & Mooney, W.D., 1995. Sesimic velocity structure and composition of the continental crust: a globe view, *J. geophys. Res.,* **100,** 9761–9788.

Churkin, M.J., Soleimani, G., Carter, C. & Robinson, R., 1981. Geology of the Soviet Arctic: Kola Peninsula to Lena river, in *The Ocean Basins and Margins, The Arctic Ocean,* Vol. 5, pp. 331–375, eds Nairn, A.E.M., Churkin, M.J. & Stehli, F.G., Plenum Press, New York.

Clark, S.A., Faleide, J.I., Ritzmann, O. & Mjelde, R., 2009. Multi-stage rift evolution of the SW Barents Sea from wide-angle seismic velocity modeling, *Geophys. Res. Abs.,* **11**(12559).

Clark, D.A., 1997. Magnetic petrophysics and magnetic petrology: aids to geological interpretation of magnetic surveys, *AGSO J. Austr. Geol. Geophys.,* **17**(2), 83–103.

Cocks, L.R.M. & Fortey, R.A., 1982. Faunal evidence for oceanic separations in the Palaeozoic of Britain, *J. Geol. Soc. Lond.,* **139,** 465–478.

Cocks, L.R.M. & Torsvik, T.H., 2011. The Palaeozoic geography of Laurentia and western Laurussia: a stable craton with mobile margins, *Earth-Sci. Rev.,* **106**(1–2), 1–51.

Dallmann, W.K. & Krasil'ščikov, A.A., 1996. Geological map of Svalbard. 1:50000, sheet D20G. Bjørnøya. Temakart 27, Norsk Polarinstitutt.

Dengo, C.A. & Røssland, K.G., 1992. Extensional tectonic history of the western Barents Sea, in *Structural and tectonic modelling and its applications to petroleum geology,* pp. 91–107, eds Larsen, R.M., Brekke, H., Larsen, B.T. & Talleraas, E., Norwegian Petroleum Society (NPF) Special Pubblication, Amsterdam.

Dibner, V.D., 1998. *Geology of Franz Josef Land,* Norsk Polarinstitutt, Oslo, 146 pp.

Dimakis, P., Braathen, B.I., Faleide, J.I., Elverhoi, A. & Gudlaugsson, S.T., 1998. Cenozoic erosion and the preglacial uplift of the Svalbard-Barents Sea region, *Tectonophysics,* **300**(1–4), 311–327.

Doré, A.G., 1991. The structural foundation and evolution of Mesozoic seaways between Europe and the Arctic, *Palaeogeogr. Palaeoelimat. Palaeoeeol.,* **87,** 441–492.

Dovzhikova, E., Pease, V. & Remizov, D., 2004. Neoproterozoic island arc magmatism beneath the Pechora Basin, NW Russia, *GFF,* **126,** 353–362.

Ebbing, J., Braitenberg, C. & Wienecke, S., 2007. Insights into the lithospheric structure and tectonic setting of the Barents Sea region from isostatic considerations, *Geophys. J. Int.,* **171**(3), 1390–1403.

Faleide, J.I., Vagnes, E. & Gudlaugsson, S.T., 1993. Late Mesozoic-Cenozoic evolution of the southwestern Barents Sea in a regional rift-shear tectonic setting, *Mar. Petrol. Geol.,* **10,** 186–214.

Faleide, J.I., Tsikalas, F., Breivik, A.J., Mjelde, R., Ritzmann, O., Engen, O., Wilson, J. & Eldholm, O., 2008. Structure and evolution of the continental margin off Norway and Barents Sea, *Episodes,* **31**(1), 82–91.

Fichler, C., Rundovde, E., Johansen, S. & Saether, B.M., 1997. Barents Sea tectonic structures visualized by ERS1 satellite gravity with indications of an offshore Baikalian trend, *First Break,* **15,** 582–585.

Forsberg, R. *et al.*, 2007. Combination of spaceborne, airborne and in-situ gravity measurements in support of Arctic Sea Ice Thickness Mapping, Danish National Space Center, *Technical Report,* **7,** 136.

Furnes, H., Ryan, P.D., Grenne, T., Roberts, D., Sturt, B.A. & Prestvik, T., 1985. Geological and geochemical classification of the ophiolitic fragments in the Scandinavian Caledonides, in *The Caledonide Orogen–Scandinavia and Related Areas,* pp. 1266, eds Gee, D.G. & Sturt, B.A., John Wiley & Sons.

Gabrielsen, R.H., Færseth, R.B., Jensen, L.N., Kalheim, J.E. & Riis, F., 1990. Structural elements of the Norwegian continental shelf. Part1: the Barents Sea Region, *Norwegian Petrol. Direct. Bull.,* **6,** 1–47.

Gardner, G.H.F., Gardner, L.W. & Gregory, A.R., 1984. Formation velocity and density—the diagnostic basics for stratigraphic traps, *Geophysics,* **39,** 770–780.

Gautier, D.L. *et al.*, 2009. Assessment of undiscovered oil and gas in the arctic, *Science,* **324**(5931), 1175–1179.

Gee, D.G., 2005. Scandinavian Caledonides (with Greenland), in *Encyclopedia of Geology,* pp. 64–74, eds Selly, R.C., Cocks, L.R.M. & Primer, I.-R., Elsevier, Amsterdam.

Gee, D.G. & Teben'kov, A.M., 2004. Svalbard: a fragment of the Laurentia margin, in *The Neoproterozoic Timanide Orogen of Eastern Baltica,* Vol. 30, pp. 191–206, eds Gee, D.G. & Pease, V., Geological Society Memoirs, London.

Gee, D.G., Bogolepova, O.K. & Lorenz, H., 2006. The Timanian, Caledonian and Uralide orogens in the Eurasian high Arctic, and relationship to paleo-continents Laurentia, Baltica and Siberia, in *European Lithosphere Dynamics,* pp. 507–520, eds Gee, D.G. & Stepherson, R.A., Geological Society Memoir, London.

Gee, D.G., Fossen, H., Henriksen, N. & Higgins, A.K., 2008. From the early Paleozoic platforms of Baltica and Laurentia to the Caledonide Orogen of Scandinavia and Greenland, *Episodes,* **31**(1), 44–51.

Geissler, W.H., 2001. Marine seismische Untersuchungen am nördlichen Kontinentalrand von Svalbard (Spitzbergen), *Unpublished diploma thesis,* Institut für Geophysik der Thechnischen Universität Bergakademie Freiberg, Freiberg.

Gernigon, L. & Brönner, M., 2012. Late Palaeozoic architecture and evolution of the southwestern Barents Sea: Insights from a new generation of aeromagnetic data, *J. Geol. Soc. Lond.,* **169,** 449–459, doi:10.1144/0016-76492011-131.

Gernigon, L., Marello, L., Barrére, C., Skilbrei, J.R. & Roberts, D., 2008. Significance of the new BAS-06 aeromagnetic survey for a better understanding of salt tectonics and basin structure in the Barents Sea, 33rd IGC International Geological Congress Oslo, Norway.

Gernigon, L., Brönner, M., Fichler, C., Løvås, L., Marello, L. & Olesen, O., 2011. Magnetic expression of salt diapir-related structures in the Nordkapp Basin, western Barents Sea, *Geology,* **39,** 135–138.

Getsen, V.G., 1991. Geodynamic reconstruction of the northeastern European part of the USSR in the Late Proterozoic, *Geotectonics,* **25**(5), 391–400.

Godfrey, N.J., Beaudoin, B.C. & Klemperer, S.L., The Mendocino Working Group USA, 1997. Ophiolitic basement to the Great Valley forearc basin, California, from seismic and gravity data: implications for crustal growth at the North American continental margin, *Geol. Soc. Am. Bull,* **108**(N12), 1536–1562.

Grogan, P., Nyberg, K., Fotland, B., Mykelbust, R., Dahlgren, S. & Riis, F., 1998. Cretaceous magmatism south and east of Svalbard: evidence from seismic reflection and magmatic data, *Polarforschung,* **68,** 25–34.

Götze, H.J. & Lahmeyer, B., 1988. Application of 3-dimensional interactive modeling in gravity and magnetics, *Geophysics,* **53**(8), 1096–1108.

Goussev, S.A. & Pierce, J.W., 2010. Magnetic basement: gravity-guided magnetic source depth analysis and interpretation, *Geophys. Prospec.,* **58**(2), 321–334.

Grad, M., Tiira, T. & Group, E.W., 2009. The Moho depth map of the European Plate, *Geophys. J. Int.,* **176,** 279–292.

Gramberg, I.S., 1988. *The Barents Shelf Platform,* Nedra, Leningrad [in Russian].

Gramberg, I.S. *et al.*, 2001. Eurasian Arctic Margin: Earth science problems and research challenges, *Polarforschung,* **69,** 3–25.

Gubaidulin, M.G., Zhuravlev, V.A. & Koifman, L.I., 1993. Profiles along the northeastern and eastern framing of the shield, in *The Structure of Lithosphere of the Baltic Shield,* USSR Acad Sci, Moscow.

Gudlaugsson, S.T. & Faleide, J.I., 1994. The continental margin between Spitsbergen and Bjørnøya, in *Seismic Atlas of Western Svalbard,* pp. 11–13, ed. Eiken, O., Nor. Polarinst. Med.

Gudlaugsson, S.T., Faleide, J.I., Fanavoll, S. & Johansen, B., 1987. Deep seismic reflection profiles across the western Barents Sea, *Geophys. J. Roy. Astro. Soc.,* **89,** 273–278.

Gudlaugsson, S.T., Faleide, J.I., Johansen, S.E. & Breivik, A.J., 1998. Late Palaeozoic structural development of the South-western Barents Sea, *Mar. Petrol. Geol.,* **15**(1), 73–102.

Guggisberg, B., Kaminski, W. & Prodehl, C., 1991. Crustal structure of the Fennoscandian Shield; a traveltime interpretation of the long-range FENNOLORA seismic refraction profile, *Tectonophysics,* **195,** 105–137.

Harland, W.B., 1985. Caledonide Svalbard, in *The Caledonide Orogen-Scandinavia and Related Areas,* pp. 999–1016, eds Gee, D.G. & Sturt, B.A., John Wiley & Sons, Chichester.

Harland, W.B. & Gayer, R.A., 1972. The Arctic Caledonides and earlier oceans, *Geol. Mag.,* **109,** 289–314.

Harland, W.B., Anderson, L.M. & Manasrah, D., 1997. The geology of Svalbard, *Geol. Soc. Lond. Memoir,* **17,** 1–521.

Hartz, E.H. & Torsvik, T.H., 2002. Baltica upside-down: a new plate tectonic model for Rodinia and the Iapetus Ocean, *Geology,* **30,** 255–258.

Henriksen, E., Ryseth, A.E., Larssen, B.G., Heide, T., Rønning, K. & Stoupakova, A.V., 2011. Tectonostratigraphy of the greater Barents Sea: implication for petroleum systems, in *Arctic Petroleum Geology,* eds Spencer, A.M., Embry, A.F., Gautier, D.L., Stoupakova, A. & Sørensen, K., Geological Society London, London.

Herrevold, T., Gabrielsen, R.H. & Roberts, D., 2009. Structural geology of the southeastern part of the Trollfjorden-Komagelva Fault Zone, Varanger Peninsula, Finnmark, North Norway, *Norwegian J. Geol.,* **89,** 305–325.

Høgden, S., 1999. *Seismotectonics and Crustal Structure of the Svalbard Region,* Geological Department, University of Oslo, Oslo, 142 pp.

Holtedahl, O., 1920. On the Paleozoic series of Bear Island, especially the Hecla Hoek System, *Norsk Geologisk Tidsskrift,* **5,** 121–148.

Hunt, C.P., Mosckowitz, B.M. & Banerjee, S.K., 1995. *Magnetic Properties of Rocks and Minerals (Vol. 3). Rock physics and phase relations: a handbook of physical constants. AGU Reference Shelf,* American Geophysical Union, 189–204.

Ivanova, N.M., Sakoulina, T.S. & Roslov, Y.V., 2006. Deep seismic investigation across the Barents–Kara region and Novozemelskiy Fold Belt (Arctic Shelf), *Tectonophysics,* **420,** 123–140.

Ivanova, N.M., Sakulina, T.S., Belyaev, I.V., Matveev, Y.I. & Roslov, Y.V., 2011. Depth model of the Barents and Kara seas according to geophysical surveys results, in *Arctic Petroleum Geology,* pp. 209–221, eds Spencer, A.M., Embry, A.F., Gautier, D.L., Stoupakova, A. & Sørensen, K., Geological Society, London.

Jakobsson, M., Macnab, R., Mayer, L., Anderson, R., Edwards, M., Hatzky, J., Schenke, H.W. & Johnson, P., 2008. An improved bathymetric portrayal of the Arctic Ocean: implications for ocean modeling and geological, geophysical and oceanographic analyses, *Geophys. Res. Lett.,* **35,** doi:10.1029/2008gl033520.

Johansen, S.E. *et al.*, 1992. Hydrocarbon potential in the Barents Sea region: play distribution and potential, in *Arctic Geology and Petroleum Potential,* pp. 273–320, eds Vorren, T.O. *et al.*, Norwegian Petroleum Society (NPF), Special Publication, vol. 2.

Johansen, S.E., Henningsen, T., Rundhovde, E., Saether, B.M., Fichler, C. & Rueslatten, H.G., 1994. Continuation of the Caledonides North of Norway—Seismic reflectors within the basement beneath the Southern Barents Sea, *Mar. Petrol. Geol.,* **11**(2), 190–201.

Kimbell, G.S., Gatliff, R.W., Ritchie, J.D., Walker, A.S.D. & Williamson, J.P., 2004. Regional three-dimensional gravity modelling of the NE Atlantic margin, *Basin Res.,* **16**(2), 259–278.

Kimbell, G.S., Ritchie, J.D. & Henderson, A.F., 2010. Three-dimensional gravity and magnetic modelling of the Irish sector of the NE Atlantic margin, *Tectonophysics,* **486,** 36–54.

Korago, E.A., Kovaleva, G.N., Lopatin, B.G. & Origo, V.V., 2004. The Precambrian rocks of Novaya Zemlya, in *The Neoproterozoic Timanide Orogeny of Eastern Baltica,* pp. 135–145, eds Gee, D.G. & Pease, V.L., Geological Society London, Memoir.

Kostyuchenko, S., Sapozhnikov, A., Egorkin, A., Gee, D.G., Berzin, R. & Solodilov, L., 2006. Crustal structure and tectonic model of northeastern Baltica, based on deep seismic and potential field data, in *European Lithosphere Dynamics,* pp. 521–539, eds Gee, D.G. & Stephenson, R.A., Geological Society, London.

Kuznetsov, N.B., Soboleva, A.A., Udoratina, O.V., Hertseva, M.V. & Andreichev, V.L., 2007. Pre-Ordovician tectonic evolution and volcano–plutonic associations of the Timanides and northern Pre-Uralides, northeast part of the East European Craton, *Gondwana Research,* **12,** 305–323.

Larsen, H.C., Saunders, A.D. & Cliff, P.D. (and the Shipboard Scientific Party) 1994. *Proceeding of the Drilling Program Initial Report*. Ocean Drill. Program, College Station, Tex, 152 pp.

Levshin, A.L., Schweitzer, J., Weidle, C., Shapiro, N.M. & Ritzwoller, M.H., 2007. Surface wave tomography of the Barents Sea and surrounding regions, *Geophys. J. Int.,* **170**(1), 441–459.

Ljones, F., Kuwano, A., Mjelde, R., Breivik, A., Shimamura, H., Murai, Y. & Nishimura, Y., 2004. Crustal transect from the North Atlantic Knipovich Ridge to the Svalbard margin west of Hornsund, *Tectonophysics,* **378**(1–2), 17–41.

Ludwig, W.J., Nafe, J.E. & Drake, C.L., 1970. Seismic refraction, in *The Sea,* Vol. 4, pp. 53–84, ed. Maxwell, A.E., Wiley-interscience, New York.

Maher, H.D., 2001. Manifestations of the Cretaceous High Arctic Large Igneous Province in Svalbard, *J. Geol.,* **109**(1), 91–104.

Marello, L., Ebbing, J. & Gernigon, L., 2010. Magnetic basement study in the Barents Sea from inversion and forward modelling, *Tectonophysics,* **493,** 153–171.

Minakov, A., Faleide, J.I., Glebovsky, V.Y. & Mjelde, R., 2012a. The structure and evolution of the Northern Barents-Kara Sea continental margin from integrated analysis of potential field, bathymetry and sparse seismic data, *Geophys. J. Int.,* **188,** 79–102.

Minakov, A., Mjelde, R., Faleide, J.I., Flueh, E.R., Dannowski, A. & Keer, H., 2012b. Mafic intrusion east of Svalbard imaged by active-source seismic tomography, *Tectonophysics,* **518–521,** 106–118.

Mjelde, R. *et al.*, 2002. Geological development of the Sørvestsnaget Basin, SW Barents Sea, from ocean bottom seismic, surface seismic and potential field data, *Norwegian J. Geol.,* **82,** 183–202.

Morozova, E.A., Pavlenkova, N.I. & Herbst, R., 2000. Ambiguity problems in constructing a seismic crustal model for the southeastern Barents Sea, *Phys. solid Earth,* **35**(2), 164–174.

Neprochnov, Y.P., Semenov, G.A., Sharov, N.V., Yliniemi, J., Komminaho, K., Luosto, U. & Heikkinen, P., 2000. Comparison of the crustal structures of the Barents Sea and the Baltic Shield from seismic data, *Tectonophysics,* **321**(4), 429–447.

Neuendorf, K.K.E., Mehl, J.P. & Jackson, J.A. (Editors), 2005. *Glossary of Geology,* 5th edn, American Geological Institute, Alexandria, VA, 779 pp.

Nikishin, A.M., Ziegler, P.A. & Stephenson, R.A., 1996. Late Precambrian to Triassic history of the East European Craton: dynamics of sedimentary basin evolution, *Tectonophysics,* **268,** 23–63.

Nystuen, J.P., Andresen, A., Kumpulainen, R.A. & Siedlecka, A., 2008. Neoproterozoic basin evolution in Fennoscandia, East Greenland and Svalbard, *Episodes,* **31**(1), 35–43.

Olesen, O., Roberts, D., Henkel, H., Lile, O.B. & Torsvik, T.H., 1990. Aeromagnetic and gravimetric interpretation of regional structural features in the Caledonides of West Finnmark and North Troms, northern Norway, *Norges geologiske undersøkelse Bull.,* **419,** 1–24.

Olesen, O., 2010. New aeromagnetic and gravity compilations from Norway and adjacent areas—methods and applications. Petroleum Geology: From mature basins to new frontiers, in *Proceedings of the 7th Petroleum Geology Conference,* pp. 559–586, eds Vining, B.A. & Pickering, S.C. *et al.*, Geological Society of London.

Olovyanishnikov, V., Roberts, D. & Siedlecka, A., 2000. Tetonics and sedimentation of the Meso- to Neoproterozoic Timan-Varanger Belt along the Northeastern Margin of Baltica, *Polarforschung,* **68,** 267–274.

O'Reilly, B.M., Readman, P.W. & Hauser, F., 1998. Lithospheric structure across the western Eurasian plate from a wide-angle seismic and gravity study: evidence for a regional thermal anomaly, *Earth planet. Sci. Lett.,* **156**(3–4), 275–280.

Ostisty, B.K. & Fedorovsky, Y.F., 1993. Main results of oil and gas prospecting in the Barents and Kara Sea inspire optimism, in *Arctic Geology and Petroleum Potential,* pp. 243–252, eds Vorren, T.O., Bergsager, E., Dahl-Stamnes, Ø.A., Holter, E., Johansen, B., Lie, E. & Lund, T.B., Norwegian Petroleum Society (NPF), Special Publication.

Otto, S.C. & Bailey, R.J., 1995. Tectonic evolution of the Northern Ural Orogen, *J. Geol. Soc.,* **152,** 903–906.

Pease, V., 2011. Eurasian orogens and Arctic Tectonics: an overview, in *Arctic Petroleum Geology,* Vol. 35, pp. 311–324, eds Spencer, A.M., Embry, A.F., Gautier, D.L., Stoupakova, A.V. & Sørensen, K., Geological Society, London, Memoirs.

Pease, V. & Scott, R.A., 2009. Crustal affinities in the Arctic Uralides, northern Russia: significance of detrital zircon ages from Neoproterozoic and Palaeozoic sediments in Novaya Zemlya and Yaimir, *J. Geol. Soc.,* **166,** 517–527.

Petrov, O.V., Sobolev, N.N., Koren, T.M., Vasiliev, V.E., Petrov, E.O., Larssen, G.B. & Smelror, M., 2008, Palaeozoic and early Mesozoic evolution of the East Barents and Kara Seas sedimentary basins, *Norwegian J. Geol.,* **88,** 227–234.

Pettersson, C., Pease, V. & Frei, D., 2009. U-Pb zircon provenance of metasedimentary basement of the Northwestern Terrane, Svalbard: implications for the Grenvilian-Sveconorwegian orogeny and the development of Rodinia, *Precam. Res.,* **175,** 206–220.

Puchkov, V., 2002. Paleozoic evolution of the East European Continantal Margin involved in the Uralide Orogeny, in *Mountain Building in the Uralides:Pangea to the Present,* pp. 9–31, eds Brown, D., Juhlin, C. & Puchkov, V., American Geophysical Union.

Ritzmann, O. & Faleide, J.I., 2007. Caledonian basement of the western Barents Sea, *Tectonics,* **26**(5), TC5014, doi:10.1029/2006TC002059.

Ritzmann, O. & Faleide, J.I., 2009. The crust and mantle lithosphere in the Barents Sea/Kara Sea region, *Tectonophysics,* **470,** 89–104.

Ritzmann, O. & Jokat, W., 2003. Crustal structure of northwestern Svalbard and the adjacent Yermak Plateau: evidence for Oligocene detachment tectonics and non-volcanic breakup, *Geophys. J. Int.,* **152**(1), 139–159.

Ritzmann, O., Jokat, W., Mjelde, R. & Shimamura, H., 2002. Crustal structure between the Knipovich Ridge and the Van Mijenfjorden (Svalbard), *Mar. Geophys. Res.,* **23**(5–6), 379–401.

Ritzmann, O., Jokat, W., Czuba, W., Guterch, A., Mjelde, R. & Nishimura, Y., 2004. A deep seismic transect from Hovgård Ridge to northwestern Svalbard across the continental-ocean transition: a sheared margin study, *Geophys. J. Int.,* **157**(2), 683–702.

Ritzmann, O., Maercklin, N., Faleide, J.I., Bungum, H., Mooney, W.D. & Detweiler, S.T., 2007. A three-dimensional geophysical model of the crust in the Barents Sea region: model construction and basement characterization, *Geophys. J. Int.,* **170,** 417–435.

Roberts, D., 2003. The Scandinavian Caledonides; event chronology, palaeogeographic settings and likely modern analogues, *Tectonophysics,* **365,** 283–299.

Roberts, D., 2007. Palaeocurrent data from the Kalak Nappe Complex, northern Norway: a key element in models of terrane affiliation, *Norwegian J. Geol.,* **87**(3), 319–328.

Roberts, D. & Gee, D.G., 1985. An introduction to the structure of the Scandinavian Caledonides, in *The Caledonian Orogeny - Scandinavia and related Areas,* pp. 55–68, eds Gee, D.G. & Sturt, B.A., John Wiley and Sons, Chichester.

Roberts, D. & Olovyanishnikov, V., 2004. Structural and tectonic development of the Timanide orogen, in *The Neoproterozoic Timanide Orogen of Eastern Baltica,* Vol. 30, pp. 47–57, eds Gee, D.G. & Pease, V., Geological Society, Memoirs, London.

Roberts, D. & Siedlecka, A., 2002. Timanian orogenic deformation along the northeastern margin of Baltica, Northwest Russia and Northeast Norway, and Avalonia-Cadomian connections, *Tectonophysics,* **352,** 169–184.

Roslov, Y.V., Sakoulina, T.S. & Pavlenkova, N.I., 2009. Deep seismic investigation in the Barents and Kare Seas, *Tectonophysics,* **472,** 301–308.

Sakoulina, T.S., Telegin, A.N. & Tikhonova, I.M., 1999. Deep seismic studies on the geophysical Zapolyarnyi-Heisa reference profile. Izvestiya, *Phys. Solid Earth,* **35,** 760–769.

Sanner, S., 1995. Et seismisk hastighetsstudium i Barentshavet, *MSc Thesis,* Geologicy Department, University of Oslo, Oslo, pp. 149.

Schmidt, S. & Götze, H.J., 1998. Interactive visualization and modification of 3D models using GIS functions, *Phys. Chem. Earth,* **23**(3), 289–295.

Schmidt, S. & Götze, H.J., 1999. Integration of data constraints and potential field modelling—an example from southern lower Saxony, Germany, *Phys. Chem. Earth,* **24**(3), 191–196.

Scott, R., Howard, J., Guo, I., Schekoldin, R. & Pease, V., 2010. Offset and curvature of the Novaya Zemlya foldand-thrust belt, Arctic Russia. Petroleum geology: from mature basins to new frontiers, in *Proceedings of the 7th Petroleum Geology Conference,* pp. 645–657, eds Vining, B.A. & Pickering, S.C., Petroleum Geology Conferences Ltd. Published by the Geological Society, London, doi:10.1144/0070645.

Sheriff, R.E., 2006. *Encyclopedic Dictionary of Applied Geophysics,* 4th edn, SEG, ISBN 1560801182, 2 pp.

Shipilov, E.V. & Vernokovsky, V.A., 2010. The Svalbard–Kara plates junction: structure and geodynamic history, *Russ. Geol. Geophys.,* **51,** 58–71.

Siedlecka, A., 1975. Late Precambrian stratigraphy and structure of the northeastern margin of the Fennoscandian Shield (East Finnmark–Timan region), *Norges Geol. Undersøkelse,* **316,** 313–348.

Siedlecka, A. & Roberts, D., 1995. Neoproterozoic sedimentation and subsequent tectonic deformation in the northern coastal areas of Norway and Russia. Norges geologiske undersøkelse, Special Publication.

Siedlecka, A., Roberts, D., Nystuen, J.P. & Olovyanishnikov, V.G., 2004. Northeastern and northwestern margins of Baltica in Neoproterozoic time: evidence from the Timanian and Caledonian orogens, in *The Neoproterozoic Timanide Orogen of Eastern Baltica,* Vol. 30, pp. 169–190, eds Gee, D.G. & Pease, V., Geological Society, Memoirs, London.

Sigmond, E.M.O. & Roberts, D. (Editors), 2007. Geology of the Land and Sea areas of Northern Europe, Special publication 10. Norges geologiske undersøkelse, 100 pp.

Skilbrei, J.R., 1991. Interpretation of depth to the magnetic basement in the Northern Barents Sea (South of Svalbard), *Tectonophysics,* **200**(1–3), 127–141.

Skilbrei, J.R., 1995. Aspect of the geology of the southwestern Barents Sea from aeromagnetic data, *NGU Bull.,* **427,** 64–67.

Slagstad, T., Barrère, C., Davidsen, B. & Ramstad, R.K., 2008. Geophysical and thermal properties of pre-Devonian basement rocks on the Norwegian continental margine, *Geol. Surv. Nor. Bull.,* **448,** 1–6.

Smelror, M., 2011. . . . .en sten løftet fra mitt hjerte. . . En reise over Polhavet i Nansens og Frams geologiske fotefar. Tapir akademisk forlag.

Smelror, M., Petrov, O.V., Larssen, G.B. & Werner, S.C. (Editors), 2009. Geological history of the Barents Sea, *Norges Geol. undersøkelse,* 1–135.

Smith, M.P., 2000. Cambro-Ordovician stratigraphy of Bjørnøya and North Greenland: constraints on tectonic models for the Arctic Caledonides and Tertiary opening of the Greenland Sea, *J. Geol. Soc.,* **157,** 459–470.

Smith, M.P. & Rasmussen, J.A., 2008. Cambro-Silurian development of the Laurentian margin of the Iapetus Ocean in Greenland and related areas, *Geol. Soc. Am. Mem.,* **202,** 137–167.

Stephenson, R.A., Yegorova, T., Brunet, M.-T., Stovba, S., Wilson, M., Starostenko, V., Saintot, A. & Kusznir, N., 2006. Late Palaeozoic intra- and pericratonic basins on the East European Craton and its margins, in *European Lithosphere Dynamics,* Vol. 32, pp. 463–479, eds Gee, D.G. & Stephenson, R.A., Geological Society, Memoirs, London.

Stoupakova, A.V., 2011. The geological evolution and hydrocarbon potential of the Barents and Kara shelves, in *Arctic Petroleum Geology,* pp. 325–344, eds Spencer, A.M., Embry, A.F., Gautier, D.L., Stoupakova, A. & Sorensen, K., Gelogical Society, London.

Torsvik, T.H., Smethurst, M.A., Meert, J.G., Van der Voo, R., McKerrow, W.S., Brasier, M.D., Sturt, B.A. & Walderhaug, H.J., 1996. Continental break-up and collision in the Neoproterozoic and Palaeozoic: a tale of Baltica and Laurentia, *Earth-Sci. Rev.,* **40,** 229–258.

Trettin, H.P., 1998. Pre-Carboniferous geology of the northern part of the Arctic islands. Chapter 4: geology of Pearya, *Geol. Surv. Can. Bull.,* **425,** 108–192.

Tsikalas, F., 1992. A study of seismic velocity, density and porosity in the Barents Sea wells (N. Norway), *(Unpublished Master Thesis),* University of Oslo, Norway.

Tulina, Y.V., Shemeleva, I.B., Sokolov, B.V., Sakulina, T.S., Nechkaev, S.A., Pavlenkin, A.D., Verba, M.L. & Nardov, N.M., 1988. Chief peculiarities of the southern part of the Barents Sea deep structure from DSS data. Geophysical Fields of Atlantic Ocean, *URSS Acad. Sci. Moscow,* 34–51 (in Russian).

Verba, M.L. & Sakoulina, T.S., 2001. The Reconstruction of the early Paleozoic structure of the Barents Sea sedimentary basin inferred from geophysical surveys along Profile 1-AR, *Polarforschung,* **69,** 85–94.

Werner, S.C., Ebbing, J., Litvinova, T.P. & Olesen, O., 2011. Chapter 11 Structural interpretation of the Barents and Kara Seas from gravity and magnetic data, in *Arctic Petroleum Geology,* pp. 197–208, eds Spencer, A.M., Embry, A.F., Gautier, D.L., Stoupakova, A. & Sørensen, K., Geological Society, London.

Ziegler, P.A., 1988. Evolution of the Arctic-North Atlantic and the Western Thethys, *Am. Assoc. Petrol. Geol. Mem.,* **43,** 1–198

Ziegler, P.A., 1989. Evolution of Larussia: a study in Late Paleozoic Plate Tectonics., Kluwer Academic Publishers, Dordrecht, 102 pp.